Characterization and Development of Novel Stationary Phases for Capillary Electrochromatography

Maria Kaltcheva

A Thesis

in

The Department

of

Chemistry and Biochemistry

Presented in Partial Fulfillment of the Requirements
for the Degree of Master of Science (Chemistry) at
Concordia University
Montreal, Quebec, Canada

April 2011

CONCORDIA UNIVERSITY

School of Graduate Studies

This is to certify that the thesis prepared

By: Maria Kaltcheva

Entitled: Characterization and Development of Novel Stationary Phases for Capillary Electrochromatography

and submitted in partial fulfillment of the requirements for the degree of

Master of Science (Chemistry)

complies with the regulations of the University and meets the accepted standards with respect to originality and quality.

Signed by the final examining committee:

____ Chair
Dr. Christine DeWolf

____Examiner
Dr. Peter Pawelek

____Examiner
Dr. Yves Gélinas

____Supervisor
Dr. Cameron Skinner

Approved by ____
Chair of Department or Graduate Program Director

April 1st 2011 ____
Dean of Faculty

Abstract

Characterization and Development of Novel Stationary Phases for Capillary Electrochromatography

Maria Kaltcheva

Porous monolithic stationary phases for capillary electrochromatography have shown great potential due to the ability to tune their properties for tailor-made separations by careful selection of the polymerization parameters. However, the final morphological and chemical properties of the column remain difficult to predict. In order to better understand the effects of the relevant variables on column properties and morphology we have significantly streamlined the preparation procedure and investigated an array of variables (temperature, reaction time, porogenic solvent concentration) on the porosity and retention of the columns. Factorial experimental design was implemented to derive models that were able to describe the polymer porosity and the retention of three PAH's as a function of starting reagents and conditions.

The current study showed that with a factorial design approach, monolith porosity and chromatography can be reliably tuned by adjusting the porogenic solvent concentration, the polymerization time and reaction temperature. Scanning electron microscopy revealed that the polymerization conditions affected the polymer structure and particle size. Synergistic effects not accessible by the "one variable at time" approach were identified between the temperature and polymerization time and temperature and monomer/porogenic solvent ratio through multivariate analysis. The control of the monolith porosity and chromatographic behaviour will allow future efforts to be focused on creating reproducible, tailor-made monolithic columns with targeted chromatographic properties suitable for the separation of peptides and proteins from biological fluids.

Acknowledgments

Many people helped me complete this work and I would like to express my gratitude to those individuals. If readers cringe at this section, but accept the rest of this work as good science, I will be thrilled!

A few people deserve special mention. Cameron Skinner has been a supportive advisor throughout my graduate and undergraduate career. He always showed faith in my work and was always encouraging and generous with his time. I read his comments on my work with a mix of gratitude (for being so detailed) and envy (why didn't I think of that?). Yves Gélinas and Peter Pawelek were great committee members who offered valuable feedback and support during many committee meetings.

Though not a member of my committee, Dirk Bandilla had a great impact on this project and offered countless suggestions, comments and edits in an effort to improve the quality of this work.

I owe special thanks to Jean-Louis Cabral as well as Jacqueline Sanchez and Rolf Schmidt for the AFM imaging data and also to Richard Allix and Aldo Dissegna for creating the numerous reincarnations of the AFM imaging device.

I would like to thank Michel Boisvert for his patience, insights and help and for teaching me how to make monoliths! I've been especially fortunate to know Adina Dobre, Angela Laroix-Fralish, Alex Lawandi, Wei Lin, Maryam Habibian and John Chin they have been great friends and their sense of humour has rescued me more times than I can recall.

I would like to thank my parents for their support through this journey. Scientists themselves, they always encouraged my quest for knowledge.

I owe special thanks to Giovanna & Orlando Panetta and the Miller-Belands for hosting me during the final months of writing.

And most of all I would like to thank Robert for his love and support and countless edits. My work is finished now and we can finally move to Europe!

Table of Contents

List of Figures viii

List of Tables x

List of Equations xi

List of Abbreviations xii

Chapter 1 Introduction 1

1.1 CEC History 1

1.2 CEC Today 2

1.3 CEC Principles 3

1.3.1 Electrophoresis 4

1.3.2 Electroosmosis 6

1.3.3 Chromatography 10

1.4 Practical aspects of CEC 13

1.4.1 CEC Instrumentation 13

1.4.2 Column 15

1.4.3 Column characterization: evaluation of conductivity and porosity 19

1.5 Effect of polymerization conditions on morphology and chromatography 23

1.5.1 Effect of Polymerization Temperature 23

1.5.2 Effect of polymerization time 24

1.5.3 Effect of porogen 25

1.6 Factorial experimental design 27

1.7 Physical Characterization: Destructive vs. Non-Destructive Methods 34

1.8 Goal 39

Chapter 2 Materials and methods 42

2.1 Reagents 42

2.2 Apparatus 43

2.3 Preparation of Monolithic Column 43

2.3.1 Pre-treatement and silanization 43

2.3.2 In situ polymerization 44

2.4 Evaluation of porosity in capillary columns 44

2.5 CEC separation of PAHs 45

2.6 CEC separation of milk proteins 46

2.7 Apparatus for Morphological and Surface Characterization 46

2.8 Scanning Electron Microscopy 48

2.9 Factorial Design Data Analysis 48

Chapter 3 Results and Discussion 49

3.1 Monolith Preparation 49

3.1.1 Capillary Silanization 49

3.1.2 Novel and simplified preparation method 52

3.2 Monolith characterization by SEM and AFM 53

    - 3.2.1 AFM 53
    - 3.2.2 SEM 57
  - 3.3 Monolith characterization by factorial design 65
    - 3.3.1 Validation of porosity measurements 66
    - 3.3.2 Chemometrics study of porosity of monoliths 68
    - 3.3.3 Chromatographic characterization of monoliths 82
  - 3.4 Application to protein separations 91
- Chapter 4 Conclusions and Future Work 98
- Appendix A: Matrix Method for Determination of b Coefficients 106
- Appendix B: SEM Images of All 27 columns 107
- Appendix C: SEM Images of UV Time Studies 110

List of Figures

Figure 1-1. Number of publications per year on CEC 2

Figure 1-2. Distribution of charges around a positively charged analyte 5

Figure 1-3. Electrical double layer near the capillary wall 7

Figure 1-4. Flow profiles in a separation column 9

Figure 1-5. Configuration of a CEC system 14

Figure 1-6. Silanization reaction on the capillary wall 17

Figure 1-7. Polymerization reaction scheme. 18

Figure 1-8. 3D representation of 2^3 factorial design 29

Figure 1-9. Iso-response plot of the reaction yield, when T = -1 (10 C). 31

Figure 1-10. Operational limitations for the analysis of pore size distribution 34

Figure 1-11. Schematic representation of AFM imaging set up. 36

Figure 1-12. Motion of the cantilever during contact mode surface scan 37

Figure 1-13. Motion of the cantilever during non-contact mode surface scan 38

Figure 1-14. Motion of the cantilever during tapping mode surface scan. 38

Figure 2-1. Custom device for imaging monoliths with AFM 47

Figure 3-1. SEM image of a capillary with failed silanization 50

Figure 3-2. AFM image in of polymer was synthesized at 20°C, 20 min, m:p1:2 54

Figure 3-3. AFM image in water polymer was synthesized at 20°C, 20 min, m:p1:2 55

Figure 3-4. Polymerization time studies 57

Figure 3-5. UV light intensity studies 59

Figure 3-6. SEM images of four main types of polymer structures 63

Figure 3-7. Graphical representation of 3^3 full factorial design 68

Figure 3-8. Porosity surface plot at 1:3 m:p 72

Figure 3-9. Normal probability plot.. 73

Figure 3-10. Predicted vs. actual porosity plot 74

Figure 3-11. Contour plot and 3D surface plot showing the effects of T,t at m:p = 1:3... 77

Figure 3-12. SEM images of all capillaries prepared with 1:3 (m:p) 79

Figure 3-13. Reduced 3^3 factorial design model... 80

Figure 3-14. Externally studentized residuals plot; 95% CI limits cut off line (in red) ... 84

Figure 3-15. Cooks distance plot with all 15 points; in red 95% CI cut off line. 85

Figure 3-16. Cook’s distance after removing Run 14 86

Figure 3-17. SEM image of 40C, 10 min,1:2 m:p mix (1 -1 -1 run 11) 87

Figure 3-18. Contour plot of k’ for pyrene 89

Figure 3-19. Separation of three PAHs and thiourea 90

Figure 3-20. Overlaid electropherograms of thiourea and model milk proteins............. 93

Figure 3-21. Electropherogram of model milk protein mixture 94

Figure 3-22. AMPS studies... 96

List of Tables

Table 1-1. Experimental matrix of 2^3 factorial design 28

Table 1-2. Experimental plan and responses of 2^3 factorial design 29

Table 3-1. Effect of silanization time on contact angle 51

Table 3-2. Porosity reproducibility tests 53

Table 3-3 Surface parameters determined by AFM (n=1) 55

Table 3-4 SEM studies of particle size 61

Table 3-5. Impact of silanization time on conductivity 67

Table 3-6. Conductivity measurements of open silanized capillaries 67

Table 3-7. Manufacturing conditions for column preparations 69

Table 3-8. Variables and Levels according to 3^3 full factorial design 70

Table 3-9. ANOVA for response surface using a two factor interaction reduced model. 75

Table 3-10. Reduced 3^3 factorial design model porosity results 80

Table 3-11. ANOVA of reduced 3^3 model 81

Table 3-12. Reduced 3^3 factorial design grid and k' results 83

Table 3-13. Model for k' using reduced 3^3 factorial design 88

Table 3-14. Milk protein properties 92

Table 3-15. Resolution of model milk proteins 95

List of Equations

Equation 1. Electrophoretic velocity μ_{ep} 5

Equation 2. Double layer thickness (δ) 6

Equation 3. Zeta potential (ξ) 6

Equation 4. Von Smoluchowski equation 8

Equation 5. Distribution coefficient (K) 10

Equation 6 Capacity factor equation (k') 11

Equation 7. Plate number (N) 11

Equation 8. Plate height (H) 11

Equation 9. Van Deemter equation 12

Equation 10. Conductivity of an open capillary 20

Equation 11. Conductivity of a packed segment 21

Equation 12 Conductivity of a packed section 21

Equation 13. Conductivity ratio of a column with packed and open segments 22

Equation 14. Archie's law 22

Equation 15. 2^3 factorial design equation for the prediction of reaction yield 30

Equation 16. Model equation for the reaction yield 30

Equation 17. Porosity model based on full 3^3 factorial design 76

Equation 18. Porosity model based on reduced 3^3 factorial design 81

List of Abbreviations

ACN	Acetonitrile
AFM	Atomic Force Microscopy
AMPS	2-Acrylamido-2-methyl-1-propanesulfonic acid
BAC	Butyl acrylate
BDDA	1,3-Butanediol diacrylate
BET	Brunauer-Emmett-Teller
BME	Benzoin methyl ether
CE	Capillary electrophoresis
CEC	Capillary Electrochromatography
HPLC	High performance liquid chromatography
ID	Inner diameter
ISEC	Inverse Size-Exclusion Chromatography
ISEEC	Inverse Size-Exclusion Electrochromatography
MTS	(3-Methacryloyloxypropyl)trimethoxysilane
OVAT	One variable at a time
PAH	polyaromatic hydrocarbons
SEM	Scanning electron microscope
THF	tetrahydrofuran
TMPM	3-(trimethoxysilyl) propyl methacrylate

Chapter 1 Introduction

1.1 CEC History

The history of capillary electrochromatography (CEC) dates back to the work of Strain who first demonstrated that higher selectivity could be obtained by applying an electric field across an absorption column in 1939 [1-2]. In 1974 Pretorius predicted that the application of an electric field across a packed column could generate a driving force, called electroosmotic flow (EOF), and if the EOF was used to drive the mobile phase instead of pressure, column efficiencies could be greatly enhanced due to the flat flow profile [3].

Early electrochromatography experiments exploiting these principles utilized columns with large internal diameters that resulted in poor heat dissipation and limited the strength of the applied electric field, resulting in low EOF and long separation times. The technique was further refined in 1981 by Jorgenson and Lukacs who used EOF-based flow in silica packed capillaries [4], demonstrating the first CEC separation. The use of capillaries with small internal diameter (50-100 μm) resulted in efficient heat dissipation, allowing higher electric fields to be employed. This allowed faster, more efficient separations with low plate heights to be achieved. The development of CEC waned through the 1980's, until the rapid growth of Life Sciences and pharmaceuticals in the 1990's created the need for miniaturized separations and enhanced separation efficiencies and peak capacities, thus reviving interest in the technique. Another reason fuelling interest was the mixed separation mechanism of CEC that has elements of both capillary electrophoresis (CE) and high pressure liquid chromatography (HPLC), leading some to speculate that CEC could potentially replace both CE and HPLC [5].

1.2 CEC Today

The tremendous interest in CEC of the previous decade has somewhat subsided, but the technique still enjoys a steady following. A search for CEC papers in Web of Knowledge shows that there has been an average of ~ 200 papers a year over the last 10 years (see Figure 1-1).

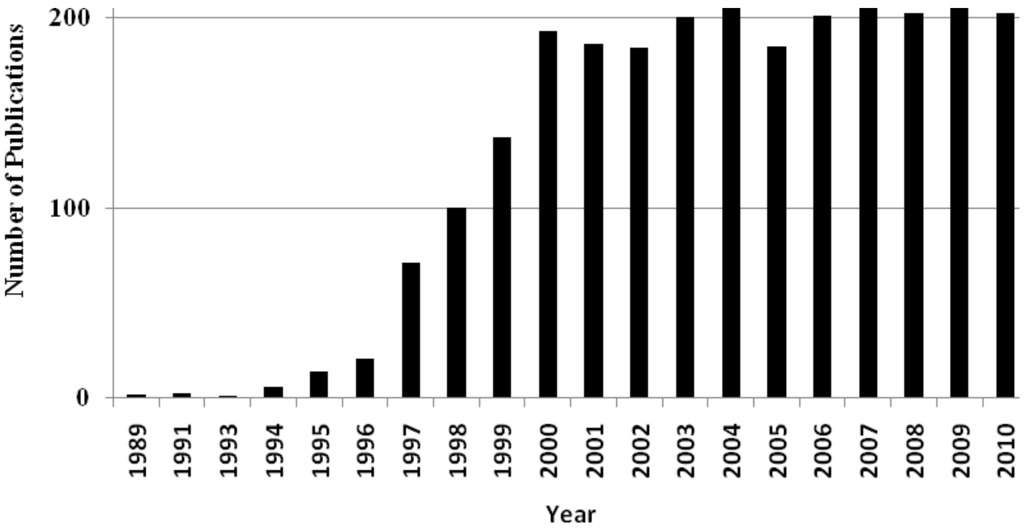

Figure 1-1. Number of publications per year from ISI Web of Knowledge using search term capillary electrochromatography

The lack of dedicated equipment and clearly demonstrated niche applications, where established methods fail, are some of the reasons for the current status of CEC [5]. Even though CEC did not meet the expectations of scientists from a decade ago with regards to applications, the technique still has a place in the lab today [5]. The steady number of publications and patents shows that scientists are still investigating the technology, exploring new applications and overcoming some of the early hurdles of the technique with the development of stationary phases that do not require frits [6-7]. The high separation efficiencies and the ability to perform difficult separations along with CE-MS interfacing are some of the reasons why researchers should continue to investigate the technique and not prematurely abandon it, despite the challenges that CEC currently faces.

1.3 CEC Principles

As is a liquid phase analytical separation technique, CEC combines the high efficiency of CE with the selectivity and sample capacity of HPLC. The laminar flow generated in HPLC is affected by fluid viscosity and flow rate. The fluid travels in parallel concentric shells or 'laminae' and the amount of friction between the column wall and the outer laminae slows down the flow near the wall, resulting in the highest velocity at the center of the column [8]. With a flat flow profile, a large selection of stationary phase functionalities and high surface area packing, CEC has several advantages over HPLC. Contrary to HPLC, where flow is achieved by applying pressure, in CEC the flow is generated throughout the column by the applied electric field.

The EOF is related to a number of physical parameters such as the permittivity and viscosity of the mobile phase, the strength of the electric field and the zeta potential, as will be explained and defined more extensively below. Separation in CEC is governed by electrophoresis, electroosmosis, size exclusion and the partitioning of the analyte between the stationary and the mobile phases. This enables the separation of both neutral as well as charged species [9]. The separation column itself can be monolithic, open tubular or particle packed, with monoliths being the most popular.

1.3.1 Electrophoresis

The process of movement of charged analytes through a solution under the influence of an applied electric field is called electrophoresis [10]. The magnitude of the analyte charge and its hydrodynamic volume determine the analyte velocity through the bulk solution towards the oppositely charged electrode; this method of motion does not apply to neutrally charged species. The mechanism is somewhat complicated by the electrical double layer that is formed around a charged solute in solution.

The double layer consists of the Stern layer and the Gouy layer. The inner Stern layer is tightly associated with the solute, while the outer Gouy layer is more diffuse and can exchange species rapidly with the bulk solution [9] (see Figure 1-2).

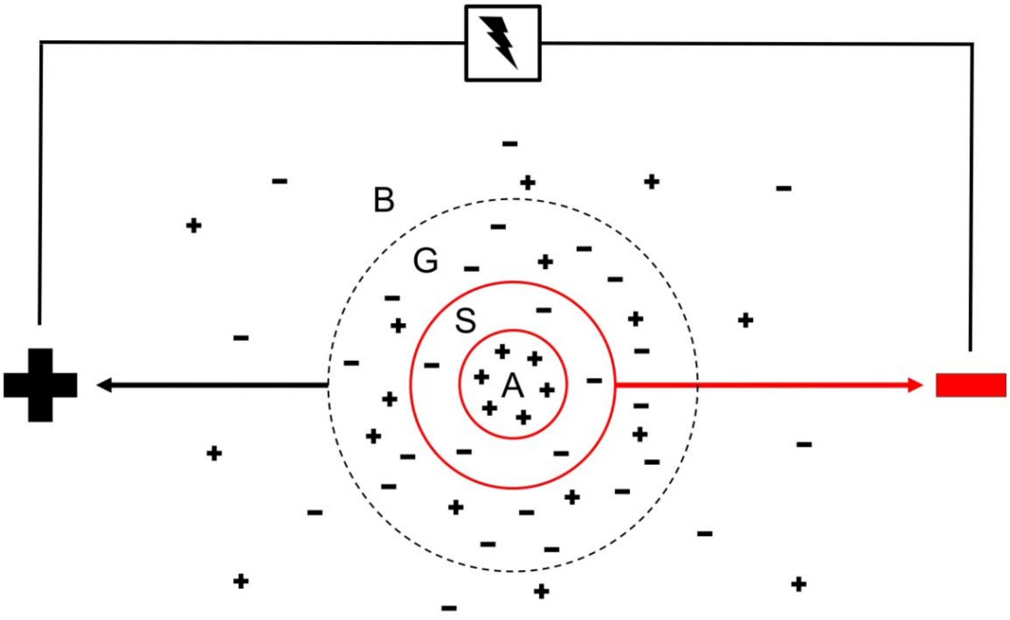

Figure 1-2. Distribution of charges around a positively charged analyte in bulk solution. (A) analyte, (S) Stern layer, (G) Gouy layer, (B) bulk solution

When this system is placed in an electric field, the analyte and its Stern layer are attracted to one electrode, while the Gouy layer is attracted to the opposite electrode. The electrophoretic velocity of an the analyte can be expressed as [9]:

$$\mu_{ep} = 0.67\frac{\varepsilon_0 \varepsilon_r \xi E}{\eta}$$

Equation 1. Electrophoretic velocity μ_{ep}; ξ is the zeta potential (*i.e.* the electrostatic potential between the bound and the diffuse layer formulated below), E is the strength of the electric field, ε_o is the vacuum permittivity, ε_r is the dielectric constant of the medium and η is the viscosity of the bulk solution

Solutes with larger hydrodynamic volumes will have a larger Gouy layer and will experience lower velocities due to the viscous drag, while solutes with higher net charge will migrate faster.

1.3.2 Electroosmosis

The EOF is generated when an electric field is applied to a capillary because of the formation of electrochemical double layers at the boundary between the charged capillary wall and mobile phase as well as between the surface of the charged stationary phase and the mobile phase. The charges on the surface attract counter ions from the mobile phase and form an electrical double layer. This double layer typically has a thickness (δ) between 1-10 nm and is expressed as [11]:

$$\delta = \left(\frac{\varepsilon_0 \varepsilon_r RT}{2IF^2} \right)^{1/2}$$

Equation 2. Double layer thickness (δ); R is the universal gas constant, F is Faraday's constant, T is the absolute temperature and I is the ionic strength of the bulk solution

The double layer is also characterized by the zeta potential (ξ), and is expressed as [11]:

$$\xi = \frac{\sigma \delta}{\varepsilon_0 \varepsilon_r}$$

Equation 3. Zeta potential (ξ); σ is the charge density at the surface

The double layer itself consists of distinct regions. The ions closest to the charged surface are tightly bound and form an immobile, rigid layer even when an electric field is applied. Further from the tightly bound layer is the diffuse layer, a region that contains large amounts of mobile counter ions in which the net charge exponentially drops to zero as the distance from the surface increases [10]. The Stern model describes this configuration and is illustrated in Figure 1-3 for a capillary but is applicable to other charged surfaces such as CEC stationary phases.

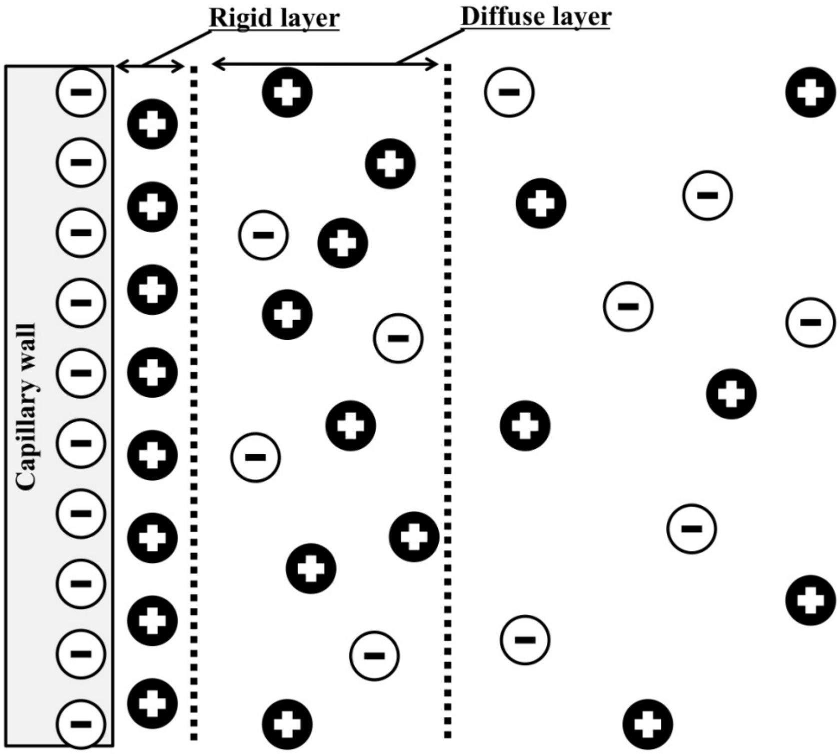

Figure 1-3. Representation of the formation of an electrical double layer near the capillary wall according to the Stern model [10]

The application of an electric field across the capillary creates a shear force along the rigid and the diffuse layers. The ions in the diffuse layer move under the influence of the force which initiates the EOF. The EOF is transmitted into the bulk mobile phase via the hydrogen-bonding network of the bulk and its direction and magnitude depend on the properties of the charged surface and the type of buffer used [12].

The flow velocity (u_{eo}) is described by the von Smoluchowski equation [13]:

$$u_{eo} = \frac{\varepsilon_0 \varepsilon_r \xi E}{\eta}$$

Equation 4. Von Smoluchowski equation; *E* is the electric field derived from the applied voltage (V) and column length (L)

The von Smoluchowski equation indicates that the EOF is dependent on the electrical double layer thickness (δ) and can be adjusted by varying the pH of the mobile phase, its viscosity and ionic strength as well as the temperature during separation. It is important to remember that the overall magnitude of the EOF is also affected by the electrochromatographic surface properties of the stationary phase, since it also carries a charge and the surface density of the charged groups, as well as their pKa's, can have a direct impact on the EOF. Furthermore unreacted, free silanol groups on the surface of the capillary wall can also influence the EOF [14].

In order to achieve efficient and reproducible separations it is important to ensure that the stationary phase can generate uniform EOF over its entire surface. When two EOF generating surfaces are in very close proximity, electric double-layer overlap can occur, that leads to the formation of stagnant non-mixing zones [15]. These EOF non-uniformities lead to excessive band broadening and lower chromatographic efficiency. The electric double-layer overlap happens at the junction between stationary phase particles or within the narrow pores of the packing material. Bartle [16] has estimated that for a typical CEC mobile phase (30/70 (%v/v) 2.5 mM aqueous buffer/ acetonitrile (ACN)), double-layer overlap would occur in pores smaller than 5 nm. At lower ionic strengths the pore size threshold for double layer overlap increases. Therefore the mean channel diameter can have significant, adverse effect when approaching the electric-double layer overlap limit [17].

As previously mentioned the EOF is generated from the entire surface which encompasses the charged stationary phase and the capillary walls. When the interstitial spaces between the stationary phase particles are sufficiently large there is no impedance to the EOF and the flow velocity in the pores of the stationary phase will be equal throughout the cross-sectional area of the column [18]. This generates the flat flow profile which is characteristic for CEC and is the reason for the high efficiency and reduced band broadening of CEC separations compared to pressure driven separations, such as HPLC (see Figure 1-4).

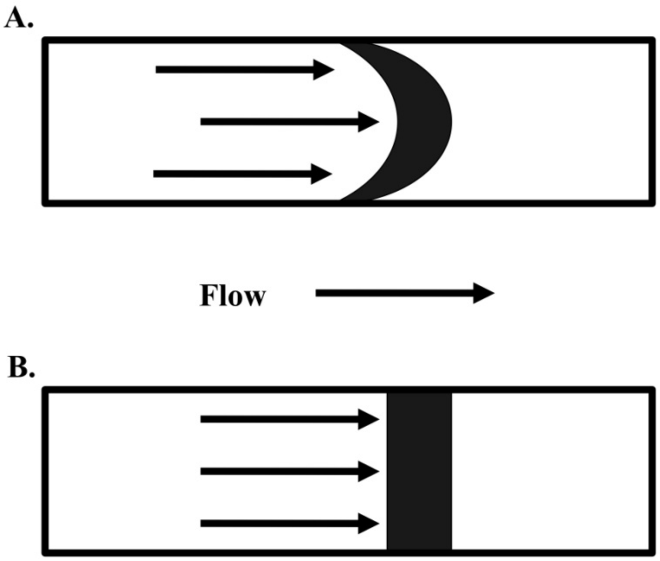

Figure 1-4. Flow profiles in a separation column induced by a pressure (A) and voltage (B)

1.3.3 Chromatography

CEC is a hybrid method that combines the high efficiency and the capillary format of CE with the selectivity and separation mechanism of HPLC. As such, CEC is a chromatographic technique, therefore general chromatographic principles apply. Chromatographic separations are based on the partitioning of analytes between the stationary and the mobile phase. Different analytes have different affinities for the stationary phase resulting in different distribution coefficients [19]. The distribution coefficient (K) is the ratio of the concentration of the analyte in the stationary phase (C_s) with respect to the mobile phase (C_M) at equilibrium and is a direct measure of the affinity of the analyte for the stationary phase relative to its affinity for the mobile phase [9].

$$K = \frac{C_S}{C_M}$$

Equation 5. Distribution coefficient (K) as a ratio of analyte concentration in the stationary phase (C_S) and concentration in the mobile phase (C_M)

The stationary phases used in CEC are similar to those used in HPLC and the same type of separation modes can be employed: reversed phase, size-exclusion, ion-exchange and affinity chromatography. In CEC the mobile phase is a mix of organic solvent (ACN or methanol) and aqueous buffer.

The capacity factor (k’) is a measure of the time the analyte spends in the stationary phase relative to the mobile phase and it quantifies the degree of partitioning between analyte and stationary phase; k' was calculated in analogy to liquid chromatography [9]:

$$k' = \frac{t_r - t_0}{t_0}$$

Equation 6. Capacity factor equation (k'), where t_r is the retention time of the analyte and t_0 is the elution time of the non-retained marker

The capacity factor is a more convenient parameter compared to the partition coefficient, because it can be calculated directly from the electrochromatogram.

The number of theoretical plates (N) can be calculated from the chromatogram using the following equation [19]:

$$N = 5.54 \left(\frac{t_r}{w_{1/2}} \right)^2$$

Equation 7. Plate number (N), where t_r is the retention time of the analyte and $w_{1/2}$ is the peak width at half height

The plate height (H) is another useful metric of column efficiency and is related to the number of theoretical plates by [19]:

$$H = \frac{L}{N}$$

Equation 8. Plate height (H) where L is the length of the separation column and N is the number of theoretical plates

The column plate height is convenient because it can be expressed as a function of experimental conditions via the van Deemter equation:

$$H = A + \frac{B}{u} + C = 2\lambda d_p + \frac{2\gamma D_m}{u} + \frac{cd_p^2}{D_m}u$$

Equation 9. Van Deemter equation where λ is a factor related to the particle shape of the packing, d_p is the particle diameter, D_m is the analyte diffusion coefficient in the mobile phase, γ the obstruction factor of the stationary phase, u is the linear flow velocity and the terms A, B and C are constants [13]

The first term (A) is referred to as the Eddy diffusion term and describes the band spreading that arises due to the different flow paths that the analyte molecules travel through the stationary phase. It is related to the homogeneity of the stationary phase packing and increases with particle size. The uniformity of the packing, the particle shape and the particle size affect the flow path and its length, which causes dispersion[20]. The second term (B) is called the longitudinal diffusion term and becomes a significant contributor to plate height at very low velocities. This term refers to the molecular diffusion that takes place in the longitudinal direction of the column and it is a result of concentration differences in the mobile phase. Both terms are related to the packing structure; the A term through λ, which is a constant that reflects the uniformity of the packing and the B term through the tortuosity factor (γ). For that reason the physical uniformity of the packing bed as well as the particle shape and diameter can have significant effect on the column efficiency [19]. The last term (C) is the resistance to mass term; it is related to the equilibrium of the analyte distribution between the stationary and the mobile phases. The resistance to mass transfer in the mobile phase is affected by the porosity (ε) because it determines the amount of mobile phase that is accessible to the stationary phase. Furthermore the column porosity affects the linear flow rate and thus influences the relative contribution of the B and C terms to the column efficiency. The EOF derived constant mixing within pores and lack of stagnant non-mixing zones leads to a much lower C term in CEC compared to HPLC, provided that no electric double layer overlap occurs.

1.4 Practical aspects of CEC

1.4.1 CEC Instrumentation

As already described, CEC is a separation technique in which the mobile phase is driven through the stationary phase using an electric field, with properties similar to both CE and HPLC. Instrumentation for CE and CEC have similar set ups and in their most simple form contain four basic elements: a power supply capable of delivering voltages up to 30 kV, a system for delivering sample/solvent to the inlet or outlet of the packed capillary, a column which has a stationary phase and a detector (UV-Vis, diode array, fluorescence, MS *etc.*). A simple sketch of a typical system is depicted in Figure 1-5.

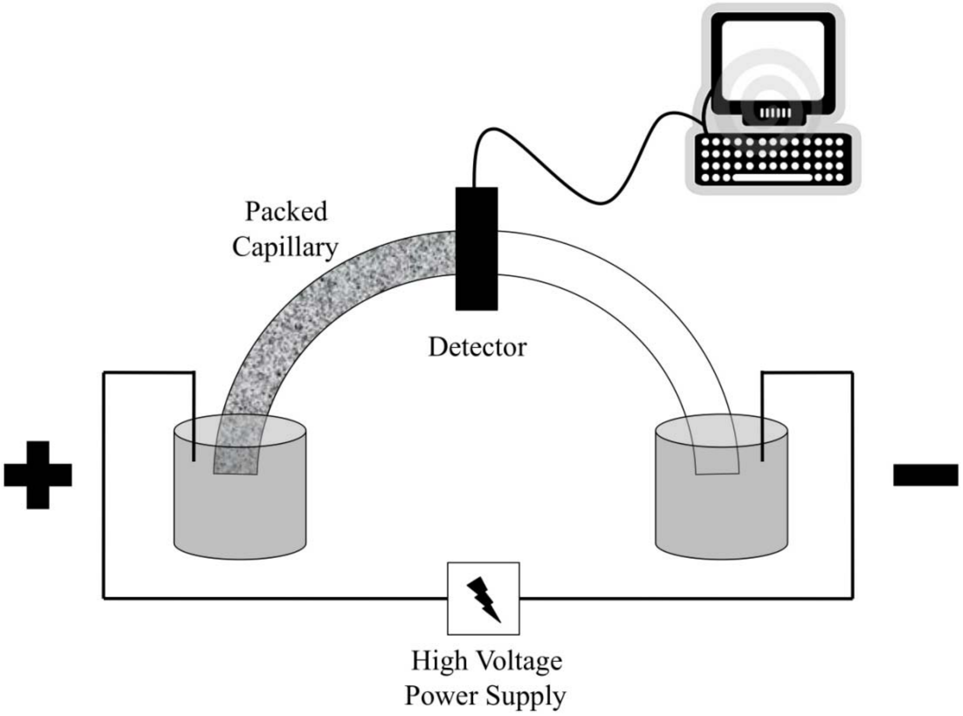

Figure 1-5. Configuration of a CEC system

Usually the capillary tube used to house the stationary phase is made of fused silica with an inner diameter of 50-200 µm, and is coated with Teflon or polyimide to impart flexibility and strength. The columns employed in CEC contain a packed and an open segment because CEC is performed on commercial CE units with minimum column length requirements that generally exceed the length of the packed segments that are typically used. In addition, these instruments require on-column detection with the detection window on the open segment. As a result, CEC columns have a packed and an open segment with a detection window located immediately after the packed section [21]. Additional features in commercial equipment include automated change of vials as well as a system to pressurize both inlet and outlet vials, to prevent air bubbles from entering the column. Reproducibility of CEC separations depends on the stringent control of experimental parameters such as temperature, voltage and pressure.

1.4.2 Column

1.4.2.1 Types of CEC columns

Reliable and reproducible column performance is critical because the column acts as the injector, pump and separation device. There are three major types of CEC columns: open-tubular (OT), particle-packed and monolithic capillary. The main drawback of OT columns is the low sample capacity caused by the low phase ratio and the low efficiency due to the high resistance to mass transfer [22]. Particulate-packed capillaries contain silica based particles, similar to those used in HPLC columns, but are kept in place with retaining frits usually prepared by sintering a small length of the particles. The difficult packing procedure, frequent bubble formation and poor column reproducibility of the particulate columns have steered researchers to develop alternative approaches [23]. Monolithic columns can overcome some of the limitations of particle-packed columns because they consist of a single network polymer structure that is covalently bonded to the capillary wall. This eliminates the need for retaining frits and has the additional advantage that small sections of the capillary can be trimmed from the inlet without destroying the entire column as they become poisoned by irreversibly bound sample components. As a result monoliths are the most widely used type of column for CEC applications [24].

1.4.2.2 Types of Monoliths

Monolithic stationary phases for CEC can be divided into three broad types: organic polymer based, inorganic (silica-based) and hybrid (organic-inorganic). Organic monoliths are further subdivided into acrylate ester-, acrylamide- and styrene-based monoliths. The high chemical and mechanical stability of methacrylate-based monoliths over a wide pH range (2 to 12) and their high efficiencies have made them attractive substrates for CEC and are widely reported in the literature [25].

The simple process for the synthesis of monolithic CEC columns usually involves modification of the capillary's silica surface with an anchoring reagent, followed by a polymerization reaction within the capillary lumen. The polymerization mixture consists of monomers, cross-linkers, porogenic (pore-forming) solvents and a polymerization initiator that is usually induced thermally or photochemically. The variety of polymerization mixtures allows a wide range of surface functionalities as well as porous properties and columns of various length and diameter can be easily prepared [24]. For a given polymerization mixture, the physical properties of the monolith are determined by the amounts, and types, of porogenic solvents, monomers, as well as the reaction conditions (*i.e.*, temperature and time).

1.4.2.3 Polymerization reaction

Our laboratory has employed a methacrylate-based monolith that was originally developed by Ngola *et al.* [26] and further refined by Bandilla and Skinner [27]. The fabrication of this monolith requires pre-treatment of the inner capillary wall with a silanization agent, (3-methacryloyloxypropyl)trimethoxysilane (MTS), via an acid catalyzed reaction (Figure 1-6).

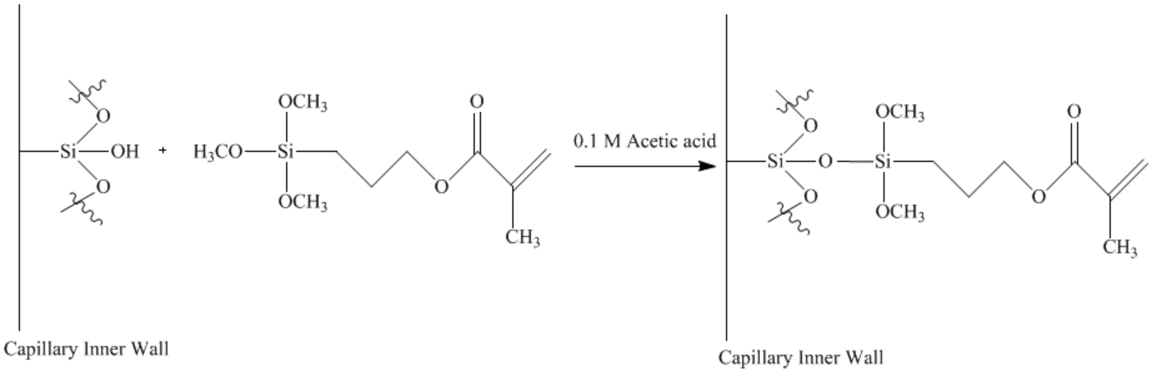

Figure 1-6. Silanization reaction on the capillary wall

This step ensures that there will be an anchor for the monolith to the capillary wall during polymerization.

The monomer mixture is then introduced into the capillary and is composed of butyl acrylate (BAC, a monomer providing butyl functionality to the stationary phase), 1,3-butanediol diacrylate (BDDA, a cross-linker), 3-(trimethoxysilyl) propyl methacrylate (TMPM, an adhesion promoter), 2-acrylamido-2-methyl-1-propanesulfonic acid (AMPS, a co-monomer providing charged functionality for EOF generation) and the photo-initiator, benzoin methyl ether (BME). The porogenic solvent consists of 60/20/20 (%v/v) mix of ACN, ethanol and 5 mM phosphate buffer, pH 7.0. The reaction proceeds according to Figure 1-7.

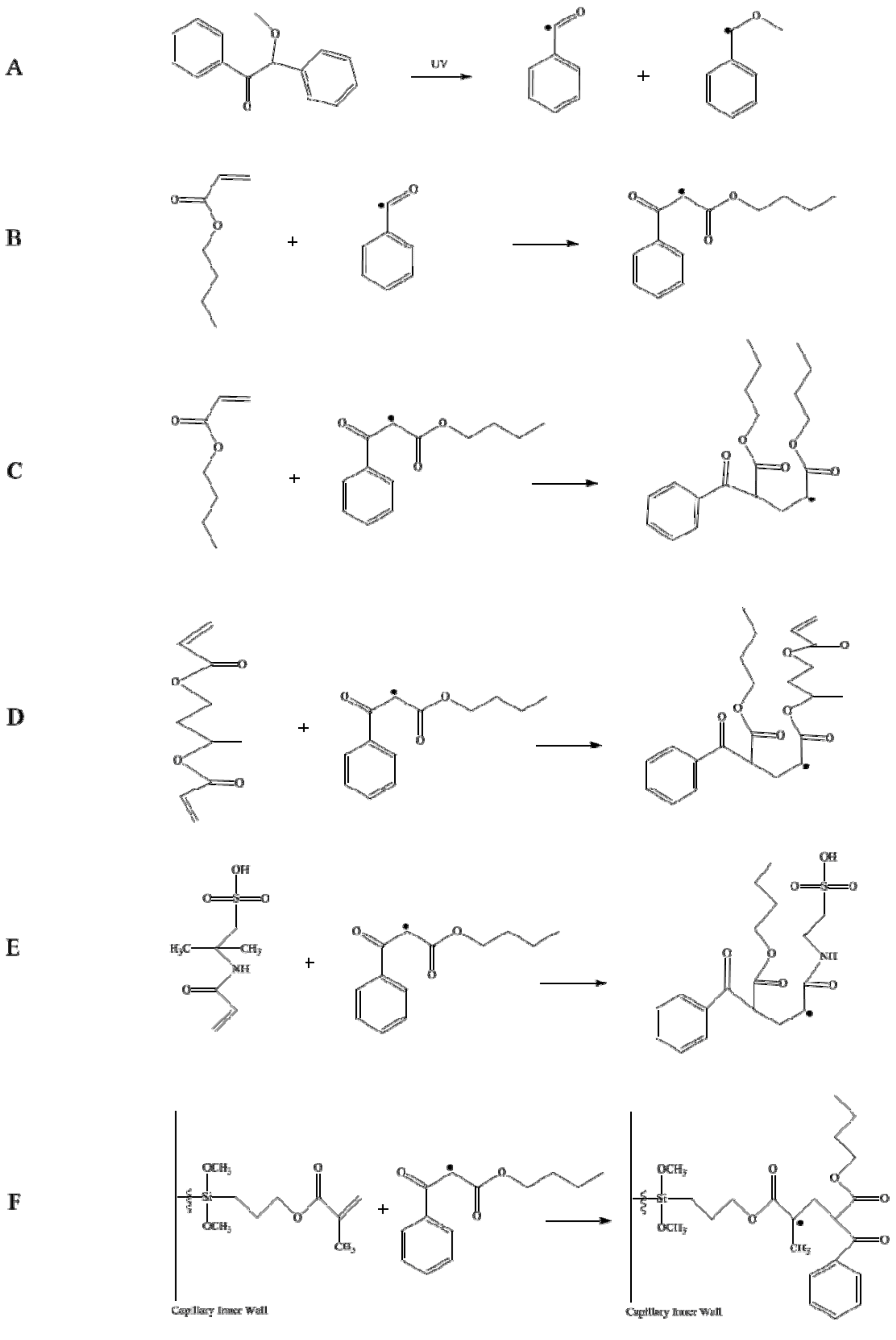

Figure 1-7. Polymerization reaction scheme. A) UV light initiation and generation of free radical B) Propagation reaction between benzoyl peroxide radical and BAC C) Propagation of BAC radical with BAC D) Propagation of BAC radical with BDDA E) Propagation of BAC radical with AMPS F) Propagation of BAC radical with the silanized capillary wall [28]

The photo initiator BME cleaves at 313 nm [29], which is within the UV transparency range of Teflon coated silica capillaries. Photopolymerization is preferred to thermally initiated polymerization because the length of the monolith section can be controlled by exposing only the desired portion of the column to the UV light.

1.4.3 Column characterization: evaluation of conductivity and porosity

It has been challenging to devise parameters for the proper characterization of CEC columns. To date, the porosity (ε) and tortuosity (γ) have been used as reliable parameters which can help assess the stationary phase wettability and the amount of stationary phase available for the CEC separation [30]. However, defining physicochemical parameters that can more adequately describe the CEC system (*e.g.*, other parameters that can predict separation efficiency and retention) and can be easily evaluated experimentally without damage to the column can lead to better understanding and help further improve the CEC process.

There are many models for the estimation of the porosity factor of a monolithic column based on gravimetric, flow and conductivity methods. Gravimetric methods measure the weight difference of columns in the presence and absence of mobile phase with known density and give a good estimate of the dead volume [30]. The flow method is based on measuring the volumetric flow rate of the solvent and the elution time of an inert tracer under controlled pressure. However, both approaches require delicate measurements that cannot be employed under CEC conditions, thus fail to give an accurate estimate of total porosity under normal operating conditions. The gravimetric method is expected to give the highest porosity because it takes into account all the void spaces within the stationary phase that are accessible to the mobile phase, while the flow method can underestimate the porosity because it relies on a tracer which has a limited diffusion in the stagnant mobile phase preventing it from exploring all the macro pores (≥500 nm diameter) and meso pores (2 nm – 500 nm diameter) [30]. The true electrokinetic porosity lies between the values obtained by the gravimetric and the flow methods. Electrical conductivity measurements have long been used to determine the porosity and permeability of geological samples [31]. The conductivity method compares the conductivity of a packed column to an identical open column under the same experimental conditions. This approach can be used to estimate the total porosity of the column under operating conditions, and is therefore a more desirable alternative to the gravimetric and flow methods [32].

It must be kept in mind that CEC columns have a packed and an open segment with a detection window between the two. Therefore, in order to measure the total porosity (ε_T) of the monolith, the conductivity of the open segment (σ_{open}) and the packed segment (σ_{packed}) must be evaluated. A simple way to estimate these values is to cut an existing column into two, fill each segment with buffer, then apply a known voltage across the segment and measure the current across each fragment.

The conductivity of an open capillary tube can be expressed as

$$\sigma_{open} = \frac{iL_o}{V_o A_o}$$

Equation 10. Conductivity of an open capillary, where L_o is the length of the open segment, V_o is the voltage applied across the open segment, A_o is the cross sectional area of the capillary and i is the current that flows through the open segment [33]

Similarly, the conductivity of the packed portion of the column can be calculated from

$$\sigma_{packed} = \frac{i' L_p}{V_p A_o}$$

Equation 11. Conductivity of a packed segment where L_p is the length of the packed segment, V_p is the voltage applied across the packed segment and i' is the current that flows through the packed section [33]

This method for evaluating conductivity is not always practical because the column cannot be re-used for chromatographic separations. Another approach for measuring conductivity that is non-destructive involves measuring the current of a regular CEC column (with both packed and open segment) and measuring the current of an open column, of the same length as the CEC column.

In this case the conductivity of the open tube is determined as above but the conductivity of the packed section can now be determined from measurements of the current across the whole CEC column as follows

$$\sigma_{packed} = \frac{i_o i_p L_p L}{V [i_o L - i_p L_o] A_o}$$

Equation 12. Conductivity of a packed section where L is the total length of the CEC column, i_o and i_p are the currents measured in the absence (open column) and the presence of the packing [33]

The ratio of conductivities of the packed and open segment can be related to the column length and the current via the following equation:

$$\phi = \frac{\left(L_p / L \right)}{\left(i_o / i_p \right) - \left(1 - \left(L_p / L \right) \right)}$$

Equation 13. Conductivity ratio of a column with packed and open segments

Then the conductivities of the packed (σ_{packed}) and open segments (σ_{open}) are related to the total porosity (ε_T) by Archie's law

$$\phi = \frac{\sigma_{packed}}{\sigma_{open}} = \varepsilon_T^m$$

Equation 14. Archie's law where ε_T is the total porosity and *m* is an empirical constant

The empirical constant m is such that when the porosity is greater than 0.2, m = 1.5 which is the typical situation in CEC where porosities range from 0.5 and 0.8. The electrokinetic porosity depends on the structure of the packing and it may not always be equivalent to the chromatographic porosity [33]. Chromatographic porosity is a geometric measurement defined as the ratio between the void space within the column and the total volume of the column, while electrokinetic porosity is a ratio of conductivities between the packed and the open segment of the column; it measures the impedance of current due to the presence of packing and is a better reflection of the experimental conditions experienced by the analyte.

1.5 Effect of polymerization conditions on morphology and chromatography

The structure of the monolith exerts a strong influence on the CEC separation by affecting the porosity and tortuosity (see Section 1.4.3). The particle size, porosity and functionality are affected by the amount and type of porogen, monomer, and cross linker, as well as the concentration of initiator and the polymerization conditions (*i.e.*, temperature and time) [34-38]. Generally the porogen is a poor solvent for the growing polymer and a good solvent for the monomers. As the reaction progresses the porogen promotes the precipitation of the polymer and formation of nuclei, which grow to the size of globules. The influence of three factors (temperature, polymerization time and monomer:porogen ratio) on monolith porosity were investigated and the effect of each of these factors on the monolith structure is discussed below. These factors were chosen because they do not change the chemical functionality of the polymer and are convenient to adjust experimentally. The monomer:porogen ratio has been shown to affect porosity, while the temperature and polymerization time have been linked to structural changes in thermally initiated systems. Very little information with regards to effect of polymerization time and temperature exists for UV-initiated systems, thus the following is mainly from what was reported for thermally-initiated systems.

1.5.1 Effect of Polymerization Temperature

Due to the connection between temperature, solubility and phase separation, the polymerization temperature is a convenient parameter that can be used to modify the morphology of the monolith because it affects the polymerization kinetically and thermodynamically. In most cases the mixing between polymer and porogen is an endothermic process and polymers are more soluble at higher temperatures. Polymers formed at higher temperatures are expected to have larger nuclei and macropores, because the phase separation occurs later and the nuclei have increased in size. However, the effect of temperature on the solvent is not always substantial and deviations from this expectation have been observed [34].

The temperature has also been observed to affect the specific surface area and pore volume of the monolith [34]. The monomers are thermodynamically better solvents for the polymer, compared to the porogen, and they solvate the primary nuclei. Polymerization continues on two fronts: within the polymerization mixture and within the monomer solvated nuclei. At low temperatures polymerization within the nuclei is kinetically preferred, however at higher temperature the secondary polymerization in solution increases. At high temperatures the secondary nuclei are captured by the growing primary nuclei and the polymer consists of larger clusters with less individualized texture and lower surface area [34]. However, it must be reiterated that these observations are made for a system that contains a thermal initiator, with much work to be done in order to more fully understand the effect of temperature in UV initiated systems.

1.5.2 Effect of polymerization time

Though it is known that the polymers growth and structure depends on the reaction time, there have been few studies on this relationship. The effect of reaction time is more easily observed in thermally initiated systems with long reaction times compared to the faster UV initiated systems. It was observed that during the early reaction stages of a thermally initiated polymerization carried out in a mold, the pore volume decreased with reaction time as did the specific surface area [35]. The pore size distribution was narrower since the largest pores disappeared as polymerization advanced [35]. To the best of my knowledge such studies have not been reported in detail on UV initiated systems.

1.5.3 Effect of porogen

In order to obtain a porous monolith, the polymerization mixture must contain a certain amount of porogenic solvent. The porogenic solvent is a binary or ternary mixture which readily solubilises the monomers, but is a poor solvent for the polymer. Varying the ratio between the constituents of the porogenic solvent changes the thermodynamic quality of the porogen, affecting the onset of phase separation and therefore the porous properties of the monolith.

Varying the amount and composition of the porogenic solvent is a commonly used method for modifying the properties of monoliths [36, 38-39]. Experiments where the proportion of porogen relative to monomers was varied revealed that when the polymerization mixture contained less monomers, the monoliths had a larger globule size and pore size. Such monoliths had lower surface area which resulted in poor column efficiency [36]. As the amount of monomers in the mixture was increased the globule size and the pore size decreased, while the column efficiency increased. This phenomenon is due to increase in the surface area of the monolith as globule size and pore size decrease. However, past a certain monomer to porogen ratio, the globule size and pore size start increasing again, resulting in low column efficiency and high column resistance to flow [36]. This shows that the effect of the proportion of porogen in the mixture on the column morphology is non-linear and needs to be optimized in order to maximize column efficiency. The decrease in the pore size for mixes with high monomer concentration can be explained by the delayed onset of phase separation due to the lower availability of porogen. Furthermore other studies have shown that the effect of the porogen on the pore size was less powerful when the porogen contained high levels of poor solvent for the growing polymer [39].

To summarize, the porous properties of the column and morphology of the polymer are controlled by the polymerization conditions; the type and amount of porogen, the amount of monomer and cross linker, the concentration of initiator and the polymerization temperature and reaction time [34-39]. To date, there are no established rules for selecting polymerization conditions and optimization experiments must be carried out for each new system. In practice, systems controlled by multiple factors have been investigated using a "one-variable-at-a-time" approach. This has been the case in the CEC literature with polymerization temperature [34], proportion of porogen, porogen composition [36-37, 40], amount of AMPS [36], polymerization time [35] having been investigated one at a time, assuming all other parameters are optimal. The major disadvantage of this approach is that it does not consider possible interactions between factors [41]. For example, it is expected that time and temperature can be related since both factors influence the kinetics of the polymerization reaction. Furthermore the temperature can affect the solubility of the monolith in porogenic solvent and thus alter the monolith structure. A more robust methodology to studying several independent factors is a factorial experimental design [42-44].

1.6 Factorial experimental design

As already discussed, the column performance and polymer structure depend on a large set of experimental factors. Traditional methods for optimization involve changing one variable at a time (OVAT) over a set experimental range, while keeping the rest of the variables constant. This approach requires a large number of experiments and generates limited information. For simple systems that are well understood and there is little or no interaction between the studied variables, the OVAT approach is still an easy and viable option of exploration of the experimental space. However, when studying complex systems that are controlled by many variables some of which may interact with one another, chemometrics offers a number of multivariate statistical tools that can reveal underlying relationships within a complex system [44].

Factorial designs are more efficient than OVAT experiments because they vary multiple factors in a coordinated strategy which ultimately requires a smaller number of experiments to characterize the system [41]. Multivariate approaches are necessary when interactions between factors are present. Models derived from the data express the relationship between the response and the variables of interest, and thus yields conclusions that are applicable to the entire experimental domain [41]. In order to obtain a model that is valid, the data in the set used to generate the calibration (training set) must meet certain requirements. The training set must be statistically representative of the unknowns on which the calibration will be used. The training set must contain all the sources of variation that are expected to be present in unknown samples. The samples used in the training set must also be mutually independent. Therefore training set samples must be prepared independently and analyzed in random order [45]. An additional data set (validation set), that is prepared and analyzed separately from the training set is used to evaluate the calibration model. It is assumed that all the variation in the response can be attributed to the variables that were used to build the model. In cases where the training set was subject to additional unquantified variables (*e.g.* instrument drift, operator error, sample aging) the model is forced to distribute contributions from the additional variable over the other variables which disrupts the proper estimate of the response [45].

The main concepts behind factorial design can be illustrated by considering a hypothetical reaction, where the yield is optimized with respect to three variables: temperature, reaction time and pH. In general, factorial designs are of the form N^k, where k is the number of variables under study (in this case T, t, pH) and N is the number of levels that each variable can take over the experimentally investigated range. This particular experiment can be performed using a 2^3 factorial design, which amounts to a total of 8 experiments. In this example, each variable is limited to two levels, (low and high), which are symbolically coded as -1 and +1. The experimental matrix and responses of a 2^3 factorial design is presented in Table 1-1and Table 1-2

Table 1-1. Experimental matrix of 2^3 factorial design

Run	Temperature (T)	Reaction time (t)	pH
1	-1	-1	-1
2	+1	-1	-1
3	-1	+1	-1
4	+1	+1	-1
5	-1	-1	+1
6	+1	-1	+1
7	-1	+1	+1
8	+1	+1	+1

Table 1-2. Experimental plan and responses of 2^3 factorial design

Run	Temperature (°C)	Reaction time (min)	pH	Yield (%)
1	10	10	5	55
2	30	10	5	53
3	10	20	5	50
4	30	20	5	40
5	10	10	10	49
6	30	10	10	46
7	10	20	10	56
8	30	20	10	49

Graphically, a 2^3 factorial design can be represented by a cube, where each point of the design space occupies a corner of the cube (Figure 1-8). For higher levels of factorial designs more points are added along the faces of the cube and inside the cube, and if there are more than 3 variables, then the design is represented by a hyper cube.

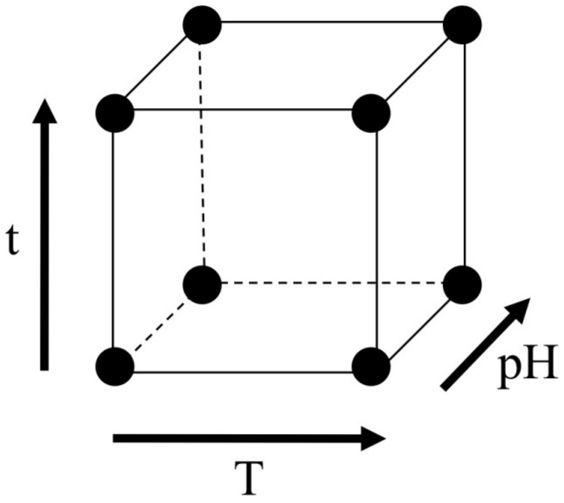

Figure 1-8. 3D representation of 2^3 factorial design

From the experimental matrix it is evident that in factorial design the factors are varied together in a coordinated way, rather than one at a time. This is why factorial design can estimate not only the main effects of each variable, but also the interaction between variables. A 2^3 factorial experiment with 8 points contains sufficient data to derive a mathematical model which can estimate a constant term (b_0) three linear terms (b_1, b_2, b_3 for each variable T, t, pH), three two-variable interactions terms (b_{12}, b_{13}, b_{23} for each pair of variables, T×t, T×pH and t×pH) and one three-variable interaction term (b_{123} for all three variables, T×t×pH) or a total of 8 variables. The model can be expressed as follows:

$$Yield = b_0 + b_1 T + b_2 t + b_3 pH + b_{12} T \times t + b_{13} T \times pH + b_{23} t \times pH + b_{123} T \times t \times pH$$

Equation 15. 2^3 factorial design equation for the prediction of reaction yield

Prior to the onset of the experiment the analyst must define the high (+1) and low (-1) levels of each variable. For the purpose of this example the yield is measured at two different temperatures (10°C and 30°C) pH levels (pH = 5 and pH = 10) and the reaction time is varied between 10 min and 20 min. The set of 8 experiments is performed in random in order to avoid introducing systematic error.

The b-terms are estimated by setting up a model matrix and taking the average of the results (see Appendix A). In this manner the general equation (Equation 15) is transformed to:

$$Yield = 49.8 - 2.8T - 1.0t - 0.3pH - 1.5T \times t + 0.3T \times pH + 3.5t \times pH + 0.5T \times t \times pH$$

Equation 16. Model equation for the reaction yield

The large negative value for the linear term of the temperature b_1 indicates that increasing the reaction temperature will lower the yield. The magnitude of the interactive terms coefficients (b_{12}, b_{13}, b_{23}, b_{123}) shows that the temperature is not involved in major interactions, therefore the negative effect of temperature on the yield will be present at any level of pH or reaction time *i.e.* temperature is independent of any other variable in the system. The t×pH interaction has a large positive coefficient ($b_{23} = 3.5$) and its impact on the yield can be visualized with an isoresponse plot of t vs. pH at the lowest level of T.

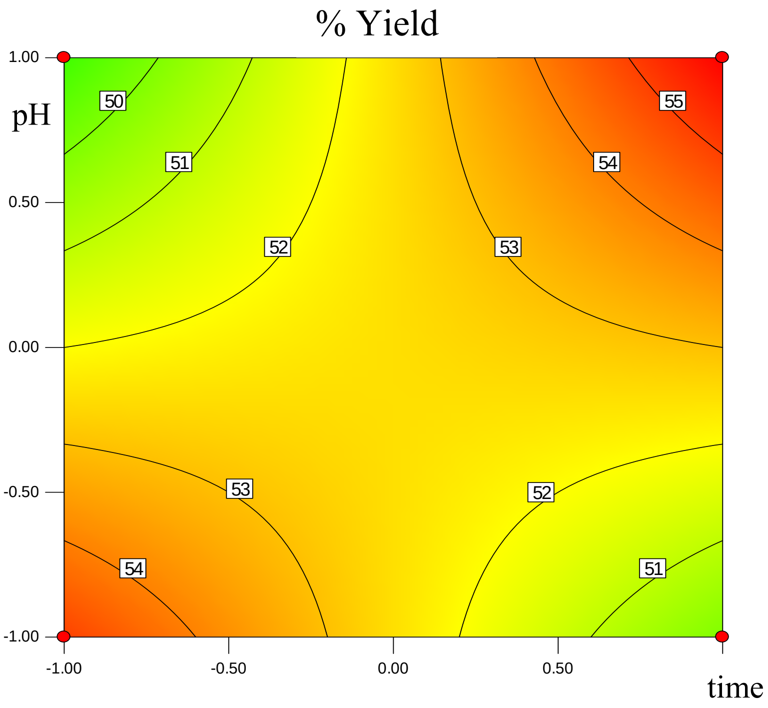

Figure 1-9. Iso-response plot of the reaction yield, when T = -1 (10°C)

The isoresponse plot in Figure 1-9 is a slice through the 3D cube across the lowest T value. In the absence of interactions, the model is linear and any slice through the design space will be a plane with parallel isoresponse curves, however, if there are interactions (as is the case in this example), the plane becomes distorted and the lines are no longer parallel. This plot clearly shows that the reaction yield will be highest whenever pH and t are both at their maximum. If this experiment was performed with OVAT and the initial starting point was in the middle of the surface, changes in pH while t is maintained at a constant level would not have had any impact on the yield. The effect of pH and t on the yield would only be evident when both are being changed at the same time due to the strong interaction present. In principle, the OVAT approach will be able to identify interactions only when the entire experimental domain is explored, which will require a large set of experiments. This example illustrated the computation of coefficient in a simple 2^3 model. Higher level factorial designs require more complex computations and are usually performed with advanced statistical software.

Factorial design is very economical method because it allows the analyst to extract a maximum amount of information about the system from a small data set compared to a similar experiment where each variable is varied individually. It can reveal the presence of interactions between the variables and provides knowledge across the entire experimental domain (within the cube), while the OVAT approach gives knowledge only in the domain where the experiment has been performed. Another benefit is that the precision of the estimate can be higher than the one obtained by OVAT [41].

The precision of the estimate from factorial design depends on two factors; the experimental variance and the leverage. The experimental variance cannot be reduced significantly since it depends on the instrument precision and the experimental error of the technician. Leverage is the potential of an experimental point to influence the values of the fitted regression model coefficients due to its position in the experimental space. In experimental systems that have error, it is beneficial to have low leverage points as this minimizes the error in the model. The maximum leverage any point can have is 1. In the case of replicate measurements the maximum leverage any replicated point can have is 1 divided by the number of replicates. A leverage of 1 would mean that the response can be predicted with a precision equal to the experimental precision, while leverage < 1 means that the response can be predicted with greater precision than if an actual experiment was performed at the same point [41]. In the OVAT approach the only way to lower the leverage (at the same level of experimental variance) is to increase the number of replicates of all points. However, the leverage obtained by factorial design is always ≤ 1 because the leverage for each point is given by p/n, where p is the number of parameters (coefficients in the model) and n is the number of experimental points. Therefore, the leverage of factorial design experiments depends only on the experimental design, it can be computed prior to the experiment and it is usually lower compared to OVAT. The variance of the prediction is the product of the leverage and the experimental variance and if the experimental variance is known it is possible to know in advance if the precision of the estimate is acceptable. In cases when it is not, the situation can be remedied much more efficiently by lowering the leverage (*i.e.* adding additional points to the model) rather than by reducing the experimental variance, which may require a more precise instrumentation/method development.

1.7 Physical Characterization: Destructive vs. Non-Destructive Methods

There are a number of physical characterization techniques for the analysis of *in-situ* prepared monoliths that have helped understand how chemistry affects monolith structure. Given that monolith structure can have great impact on chromatographic behaviour these techniques are often used for the evaluation of novel stationary phases. Mercury intrusion porosimetry (MIP) and gas sorption (Brunauer-Emmet-Teller (BET), Barrett-Joyner-Halenda (BJH) can provide a great deal of information about the pore size distribution, especially when used together as complementary techniques. Generally MIP is good for the upper range of pore sizes and allows for the determination of macropores whose width > 50 nm, with gas adsorption performing best in the lower size range (mesopores, 2 nm < width < 50 nm), while micropores (width < 2 nm) are usually inaccessible and are difficult to characterize (Figure 1-10).

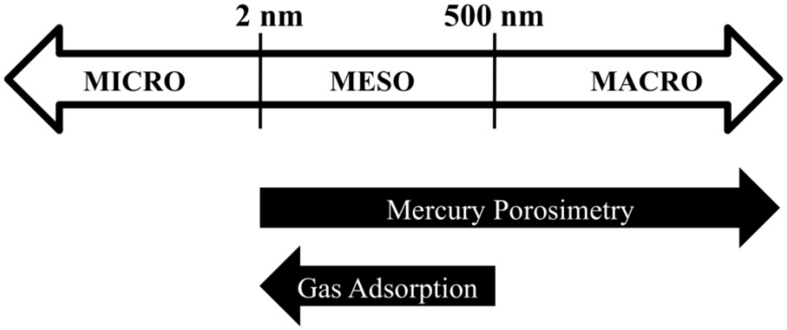

Figure 1-10. Operational limitations for the analysis of pore size distribution

The main drawback of these techniques is that they require a large mass polymer sample that must be formed in bulk, and therefore may not be directly comparable to the polymer that is cast inside a capillary. Bulk polymerization is subject to vertical gradient effects that are due to the ability of the UV light to penetrate the solution, furthermore as polymerization progresses the nuclei settle on the bottom of the solution and the overall structure is not completely uniform. Due to the small diameter of the capillary (100 µm) such directional non-uniformities are not present. In addition, MIP, BET and BJH are destructive methods and the sample that has been characterized cannot be used in other analyses. While the results of these techniques give a good estimate of the overall range of pore sizes they are not always a good predictor of chromatographic behaviour because the analysis cannot be performed under the wetted conditions that are used in chromatography [46].

There are chromatography based techniques such as Inverse Size-Exclusion Chromatography (ISEC) and Inverse Size-Exclusion Electrochromatography (ISEEC) that are non-destructive and can evaluate porosity under chromatographic conditions. The methods are based on the study of the retention of molecular probes with known sizes that have access to the whole stationary phase and are not limited to the surface (unlike MIP, BET, and BJH). The drawback of this approach is the limited size range of available probes and the necessity of using non-retentive operating conditions that requite strong solvents such as tetrahydrofuran (THF) which are not compatible with CEC polymers and are thus not suitable for this work [47-48].

Monoliths are often studied by SEM in the dry state even though the resolution limit of 50 nm is not sufficient for detailed structural study. It is a relatively simple technique that offers a good estimate of the overall macro structure of the polymer. Imaging by SEM does not require a large amount of sample and the polymer can be imaged as cast within the capillary. For best results the sample should be relatively flat and conductive, which can be achieved by sputtering a thin layer of Au-Pd on the surface.

Unfortunately, the highly reticulated surface of the polymer as well as its thermal sensitivity that can limit the voltage applied during imaging and can reduce the image resolution, but nonetheless SEM remains one of the most popular methods for analyzing novel monolithic phases [26, 32, 49].

Similarly to SEM imaging, AFM is a technique that is also employed for the study of surface topography. This type of imaging is based on a raster scan of the sample surface by a flexible cantilever that probes the surface with a very sharp tip [50].

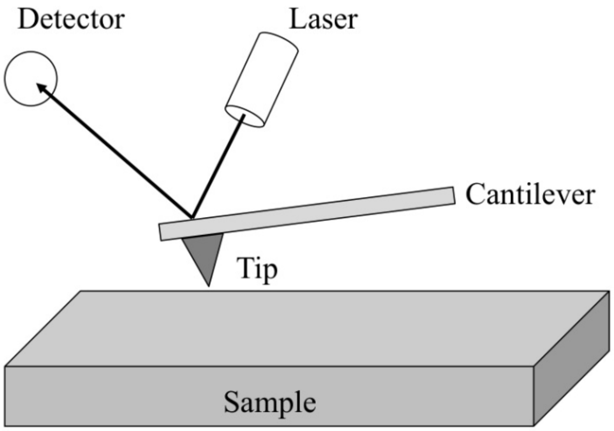

Figure 1-11. Schematic representation of AFM imaging set up

The AFM tips are made of Si or Si_3N_4 and can have a radius as small as 5 nm. During the scan, a laser beam focused on the back of the cantilever is reflected to a photodiode detector (Figure 1-11) and surface-tip interactions cause variations in the reflections which are recorded as the tip scans the sample. Chemical modification of the AFM tip with a reactive group has been employed to map the reactivity of surfaces. However, this chemical imaging was not employed here since the primary interest was to study the monolith topography.

The AFM is able to image samples in air as well as in wetted state, which makes it very suitable for investigating the properties of monoliths under chromatographic conditions. The high resolution 3D surface images achieved with AFM give superior surface depth resolution compared to SEM and thus can be a better tool for the estimation of the surface roughness.

There are three main operational modes: contact mode, non-contact mode, and intermittent contact (tapping) mode. In contact mode the tip is dragged along the surface and the topography of the surface is measured by the deflection of the cantilever (Figure 1-12). This mode of scanning is best suited when the overall interactive force between the sample and the tip is repulsive.

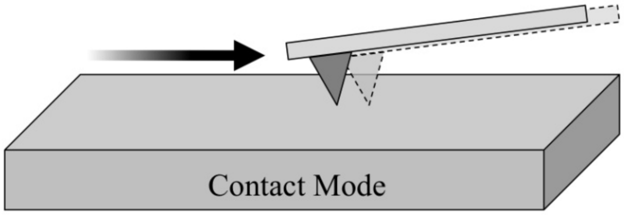

Figure 1-12. Motion of the cantilever during contact mode surface scan

When there is significant interaction between the tip and the sample, the cantilever can be oscillated in order to minimize these effects. In non-contact mode a stiff cantilever is oscillated close to the sample surface without touching it (hence, “non-contact”, Figure 1-13). The frequency and amplitude of the oscillating probe changes when the tip approaches the surface due to van der Waals interactions, these changes are recorded and used to generate the topographic image.

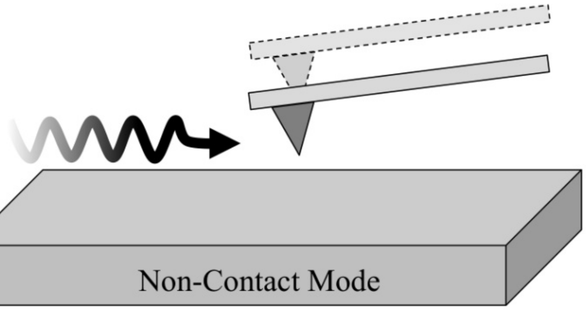

Figure 1-13. Motion of the cantilever during non-contact mode surface scan

Tapping mode is suitable for the imaging of soft samples because it applies less force and is less damaging (Figure 1-14). It is similar to non-contact mode in that a stiff cantilever is oscillated, but this time the tip is closer to the surface and intermittently touches it. This mode can be used for imaging in the wetted state and can achieve high resolution for very fragile or soft samples.

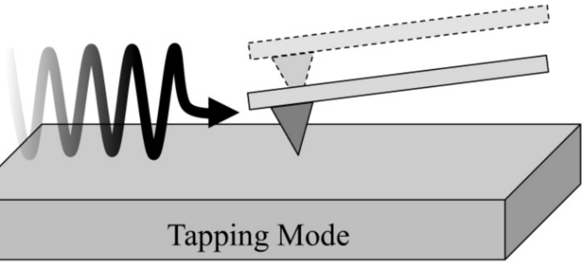

Figure 1-14. Motion of the cantilever during tapping mode surface scan

The technique, however, is not facile and to obtain a single image can be quite laborious. Selecting the proper AFM imaging conditions can be a lengthy process particularly when the sample is very soft as is the case with monoliths. In many cases the sample is usually dried prior to analysis and some shrinkage is expected [51], however the particle and pore sizes obtained by SEM and AFM were comparable [46]. A study of a photo-polymerized methacrylate-based monolithic stationary phase was performed in three solvent systems: water, ACN and 50/50 (% v/v) ACN/water by Cabral *et al.* The liquid AFM images revealed that the polymer contracts in water, suggesting that the monolith particles have a higher density of hydrophobic (butyl), than hydrophilic (sulfonate) functionalities on their surface [46]. Liquid AFM imaging is a great tool for direct analysis of the swelling process of stationary phases with respect to different solvents. However, the naturally convoluted structure of monoliths limits the studied area only to the surfaces that are relatively flat and on the top face of the monolith. The minimum accessible pore size depends on the tip radius and thus only macro- and meso-pores can be reliably probed [46]. Furthermore any structural changes that are observed could be due to the inherent heterogeneous structure of the monolith and the fact that different parts of the polymer are imaged each time. This makes the interpretation of any observed changes difficult. However, combining results from imaging techniques with electrokinetic and chromatography-based techniques could lead to a better understanding of monoliths and result in the development of methods for better tailoring of their chromatographic properties.

1.8 Goal

The goal of this project was to study the influence of key variables such as temperature, UV irradiation time and amount of porogenic solvent on the porosity and the chromatographic behaviour of CEC monolithic columns. Studies of the pore size distribution of the monolith by BET conducted previously in our lab suggest that the majority of the pores have a diameter of 20 nm or less [28]. Previous work by our group suggests that the monolith would be better suited for small proteins and protein digest separations if the size of the pores is ~30 nm; mesopores with that diameter are the major sites of interaction between proteins and the stationary phase. The pore structure of the stationary phase determines the surface area available for the separation. Apart from influencing the overall surface area, the pore size also limits the size of the analyte since pore diffusion is related to the efficiency of the column via the mass transfer term in the van Deemter equation. In order to ensure sufficient surface area, while providing a wide enough pore diameter to facilitate mass transfer the analyte size must be 5-15% of the pore size. Therefore small protein digests (1-20 kDa) are best suited for pores of 30 nm.

In order to increase the size of the mesopores different polymerization conditions were explored using a factorial experimental design, AFM and SEM imaging for characterization and finally CEC separation of polyaromatic hydrocarbons (PAH) to characterize the chromatography. Previous studies have shown that polymerization conditions have an impact on the chromatography and porosity of monoliths [38-39]. In this study three variables were chosen to develop a three-factor (polymerization time (t), temperature (T) and monomer: porogen ratio (m:p)), three-level factorial design (3^3). A three level design will result in a quadratic function, which allows the detection of interactions between variables; a two-level design will result in a linear function, which is insufficient, while a four-level design requires more runs and results in a cubic function, useful when more complex interactions are under investigation. If medium values are missing from the design, the method will attempt to minimize error for points at the vertices thus introducing greater error in the central region of the design space. This error can be significant, especially when nonlinear interactions are present. Including medium-level points in the design ensures that the model does not attempt to minimize errors at the vertices at the expense of the central region

Factorial design was used to determine whether t, T and m:p were independent of one another and how polymerization conditions affected the structure and chromatography of CEC columns with respect to PAH separations. The resultant equations were intended for eventual formalization as a predictive synthetic model applicable to CEC column preparation.

Chapter 2 Materials and methods

2.1 Reagents

Benzoin methyl ether (BME) was obtained from Fluka (Sigma–Aldrich, Oakville, Canada), (3-Methacryloyloxypropyl)trimethoxysilane (MTS), butyl acrylate (BAC), 1,3-butanediol diacrylate (BDDA), 2-acrylamido-2-methyl-1-propanesulfonic acid (AMPS), thiourea, acenaphthene, pyrene, fluoranthene, sodium tetraborate, dibasic sodium phosphate, ethanol, α-lactalbumin, β-cassein and κ-cassein were purchased from Sigma–Aldrich (Oakville, Canada). HPLC grade ACN and methanol were acquired from Fisher (Napean,Canada), glacial acetic acid was obtained from J.T. Baker (Phillipsburg, NJ, USA). All organic solvent buffers were filtered through 0.45 μm Whatman nylon membrane filter, while all aqueous buffers were filtered through 0.45 μm Millipore mixed cellulose ester filter. The solutions were prepared fresh on a monthly basis and stored at 4°C and degassed by sonication under vacuum prior to use.

Concentrated protein stock solutions of α-lactalbumin, β-cassein and κ-cassein were prepared in water and were frozen at – 80°C. The solutions were prepared fresh daily by thawing the stock solution and diluting with 50/50 (%v/v) mix of 5mM borate, pH 10 and ACN prior to injection.

Stock solutions of polyaromatic hydrocarbons (PAH) were prepared in 20/80 (%v/v) mix of 5mM borate, pH 10 and ACN. All buffers and aqueous sample solutions were prepared using ~18 MΩ deionized water (NANOpure, Barnstead, Dubuque, IA, USA).

2.2 Apparatus

Porosity experiments were conducted using a laboratory-built CEC instrument. Voltage was applied using a Spellman Model CZE 1000R high-voltage power supply (Happauge, NY, USA) and current was measured via a current to voltage resistor at 20 Hz with a PCI-1200 (12 bit resolution) data acquisition board (National Instruments, Austin, TX, USA).

CEC separations of PAHs and model milk proteins were performed with a P/ACE MDQ CE System with a diode array detector (DAD) and data was analyzed with Karat 32 software V. 5.0 (Beckman Coulter, Fullerton, CA, USA). The cooling system was bypassed since the coolant was found to damage the Teflon coating of the capillary.

2.3 Preparation of Monolithic Column

2.3.1 Pre-treatement and silanization

Teflon coated fused-silica capillaries (100 µm I.D. 365 µm O.D.) were purchased from Polymicro Technologies (Phoenix, AZ, USA). Capillary columns were treated successively with ethanol, 1 M sodium hydroxide and water, then (~ 50 column volumes) of freshly prepared solution containing 50/30/20 (%v/v) ethanol, glacial acetic acid and MTS were passed through the capillary and the filled capillary was sealed at the ends for 12 hrs. Following silanization, the capillaries were washed consecutively with methanol and water and dried under a stream of N_2 for 30 minutes.

2.3.2 In situ polymerization

The monomer mixture was composed of 3.0 mg AMPS, 15.0 mg BME, 150 μL BDDA, 340 μL of BAC and 1.5 μL of MTS. The porogenic solvent consisted of 60/20/20 (%v/v) ACN, ethanol, and 5 mM phosphate buffer, pH 7.0. The monomers were mixed with the porogenic solvent to the desired ratio (1:2, 1:3 or 1:4 monomer mix: porogenic solvent (v/v)) and the polymerization mixture was kept frozen at -80 ^{o}C. The mix was thawed then vortexed for 5 min. The capillaries were filled with polymerization mixture and 10 cm was exposed to UV light for 10, 20 or 30 min under a high-pressure mercury lamp (GE 175 Watt). Output at 50 cm below the lamp was 1.8 W/cm^2 as measured with an Indicator Model 154BT power meter (Laser Instrumentation, Cherttosey, UK). During the polymerization reaction the capillary was placed on an aluminum sheet in an ice bath (0°C), in a hot water bath (40°C) or at room temperature (20°C). Following the polymerization step excess monomers were purged from the packed columns with ACN at 100 psi for 1 h. Lastly, the capillary was conditioned for 30 min at 10 kV, 6.9 bar (equivalent to100 psi, which was instrumental maximum) and then for another 30 min at 10kV with the desired mobile phase. Prior to each run, the capillary was conditioned for 8 min with voltage and pressure and for 5 min with voltage only.

2.4 Evaluation of porosity in capillary columns

Conductivity measurements of packed columns were carried out on the lab-built CEC system by filling the CEC column and an open silanized capillary of exactly the same length with 50/50 (%v/v) ACN and 5 mM, pH 10 borate buffer and measuring the current in each capillary at 8 kV. The column was conditioned until a stable current was obtained, typically within 30 min. The current for the packed column (i_p) and open capillary (i_o) were recorded and the conductivity ratio (ϕ) was obtained using Equation 13. The total porosity (ε_T) was calculated from the conductivity ratio according to Equation 14 [52].

2.5 CEC separation of PAHs

Separations by CEC were carried out on the P/ACE MDQ CE System modified to bypass the coolant. The columns were conditioned with 80/20 (%v/v) mobile phase of ACN and 5 mM borate pH 10 by applying 8 kV for 30 min at 6.9 bar at the outlet vial. This long equilibration step was performed only after manufacturing the capillary in order to remove the ACN that was used to remove any unreacted monomers. This was followed by electrokinetic conditioning at 8 kV, 0 bar for 30 min to achieve a stable current. This step was necessary in order to condition the monolith with the mobile phase that was used during the PAH separations.

Prior to each injection a similar but shorter equilibration step was performed (8 min 8kV 6.9 bar, 5 min 8 kV 0 bar). Injections were done electrokinetically for 2 sec at 5 kV. Separation was performed at 8 kV with 1 psi on both inlet and outlet vial. All experiments were performed at room temperature in reverse polarity mode. The length of the packed section was 10 cm and the total length was kept at 30.5 cm. The packed segment of the capillary was placed at the outlet, so that the detector window was immediately after the packed section.

2.6 CEC separation of milk proteins

Milk protein separations were carried out on the P/ACE MDQ CE System, that was modified to bypass the coolant. Prior to first use, the columns were conditioned with 50/50 (%v/v) mobile phase of ACN and 5 mM borate pH 10 by applying 8 kV for 30 min at 6.9 bar at the outlet vial. This equilibration step was performed only when change of solvent was required. This step was followed by 30 min electrokinetic conditioning at 8 kV, 0 bar until a stable current was achieved.

Between injections a shorter equilibration step was performed. The column was flushed for 8 min at 8kV with pressure of 6.9 bar, followed by electrokinetic conditioning for 5 min at 8 kV without pressure. Sample injections were performed electrokinetically for 2 sec at 5 kV. During the separation, pressure of 0.07 bar was applied on the inlet and outlet vials. The separations were performed at ambient temperature in reverse polarity mode. The length of the packed section was 10 cm and the length of the open segment was 20.5 cm, making up for a total of 30.5 cm.

2.7 Apparatus for Morphological and Surface Characterization

AFM experiments were conducted and analyzed with a Nanoscope V Dimension 3100 AFM instrument. Images acquired in air in tapping mode used NCR Arrow probes at 1.21 Hz, images acquired in water (Milli-Q, 18.2 MΩ.cm) in tapping mode used MicroLever E probe at 0.748 Hz scan rate. The step size was 2 µm in air and 3µm in water. The images were acquired at ambient temperature. A 5 µm × 10 µm segment was imaged in air and a 20 µm × 10 µm section was imaged in water at 384 × 192 resolution.

Different sections of the same column were used for the images in air and in water. Several areas were imaged under each condition.

A custom made aluminum block with a magnet puck attached to the bottom was used to hold the capillary upright for AFM imaging

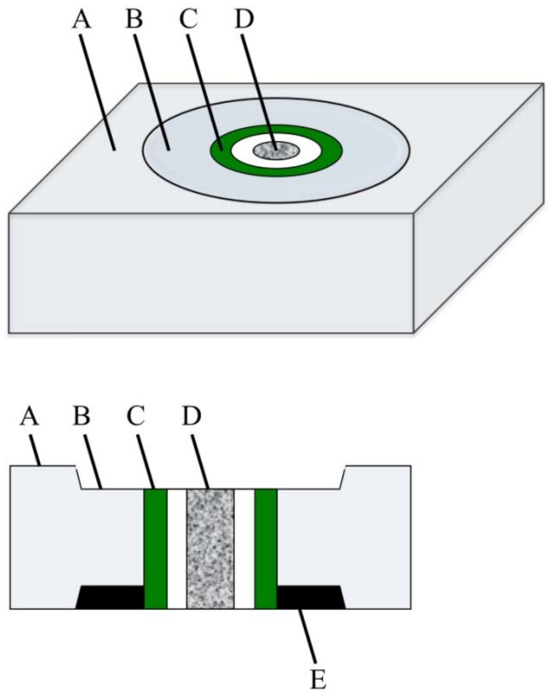

Figure 2-1. Top view and cross section of a custom device for imaging monoliths with AFM; A) Aluminum block B) Trough C) PEEK tubing D) Capillary with monolith E) Magnet puck

The aluminum block had a hole with (1/16" diameter) through which a gray PEEK tubing (ID: 0.015", Upchurch Scientific) was threaded. The capillary was placed inside the PEEK tubing and the monolith within the capillary was imaged directly in air and in water. A shallow trough on the top of the aluminum block was made in order to contain water during liquid imaging.

2.8 Scanning Electron Microscopy

The monoliths were prepared as previously described in sections 2.3.1 and 2.3.2. The capillaries were cut to a length of ~ 1 cm and placed on sticky carbon tape attached to aluminum stubs then coated with ~200 Å Au/Pd with Hummer VI Au-Pd Sputter Coater. The monoliths were imaged with Hitachi S-3000N Variable Pressure-SEM (VP-SEM) at 15.0 kV.

2.9 Factorial Design Data Analysis

The experiments were carried out in a 3^3 full factorial design set up. The variables explored in the design were the monomer:porogen ratio, the polymerization temperature and time. The total porosity was the response variable. Design-expert v.8 software was used to evaluate both major and interactive effects.

Chapter 3 Results and Discussion

This chapter is organized into four sections. First, results of the preparation of the polymers and a novel monolith preparation method are presented and discussed. Images of polymer in water and air by AFM are shown along with SEM images of monoliths synthesized under different polymerization conditions. Following this are the results from the chemometric analysis of porosity and chromatography with respect to synthetic conditions. Finally, the application of CEC columns to protein separations is discussed.

3.1 Monolith Preparation

3.1.1 Capillary Pretreatment and Silanization

Prior to the synthesis of the monolith, the capillary had to be pre-treated with NaOH in order to activate the silanol groups on the capillary wall. Following this pre-treatment, a silanization step was performed in order to form a Si – O – Si – C bond between the capillary wall and the reactive pendant methacrylate group of TMPM (See Section 2.3.1). These pendant methacrylate groups further reacted with the radicals in the polymerization mixture and covalently anchored the monolith to the wall. Failure to silanize the wall caused the monolith to detach, and resulted in poor separation (See Figure 3-1).

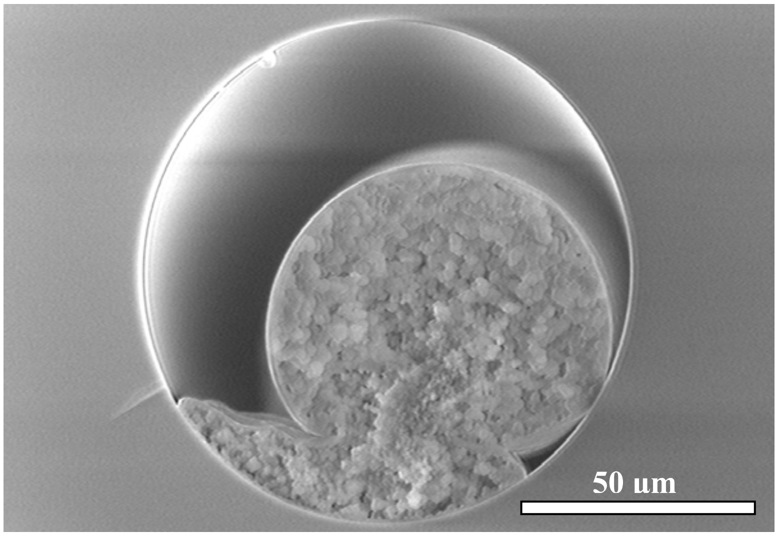

Figure 3-1. Cross sectional SEM image of a capillary with failed silanization at 700x magnification

Thus it was important to have a convenient way of determining whether silanization was achieved or not. Such a method was developed by Huang and Horvath and involves measuring the contact angle of the capillary wall [53]. The contact angle could be related to the hydrophobicity of the capillary wall. The addition of methacrylate groups from TMPM after silanization made the inner surface of the capillary more hydrophobic, compared to an untreated capillary. The more hydrophobic surface resulted in a higher contact angle. This effect levelled off when silanization was complete and no further addition of methacrylate groups was possible.

In the method formally used in our lab, the silanization was performed with a 50/30/20 (%v/v) mix of water, glacial acetic acid and TMPM. However it was observed that TMPM did not readily dissolve and after a short period of time the mixture underwent phase separation, even with thorough homogenization prior to injecting into the capillary. This potentially caused a non-uniform coating of the wall and/or non-uniform binding of the monolith that degraded separation efficiency and resulted in poor column-to-column reproducibility. In an effort to avoid this issue, water was replaced by ethanol in the reaction solvent, while the proportions were kept identical (*i.e.*, ethanol/glacial acetic acid/TMPM 50/30/20 (%v/v)) to the previously used silanization mixture. No phase separation was observed with the new solvent regime, so uniform silanization was expected to occur. To confirm uniform silanization, the contact angle was measured and it was concluded that the reaction was complete after 1 hour since no further change in the contact angle was observed after that amount of time (Table 3-1). The contact angle for fused capillary was comparable to the one reported by Huang and Horvath, but there was a difference between the contact angle for the silanized capillary reported here (56°) and that reported by Huang and Horvath (75°). This could be attributed to differences in the type of silanization mixture, which resulted in a higher coverage of the capillary wall with methacrylate. In addition, the silanization in this work was performed at ambient conditions instead of 120°C for 6 hrs [53].

Table 3-1. Effect of silanization time on contact angle

silanization time (hrs)	**contact angle (θ) (deg)***
0**	25 ± 3
1	55 ± 5
2	51 ± 3
4	59 ± 2
8	59 ± 4
24	55 ± 3
avg	***56 ± 3***

*n=3

**fused silica treated with NaOH and dried under N_2

3.1.2 Novel and simplified preparation method

The method for polymer preparation previously employed in our lab required several lengthy steps that sometimes resulted in poor chromatographic reproducibility of the columns. Briefly, inhibitors added to the highly reactive monomers by the manufacturers were removed by adding Amberlite resin and stirring the mixture overnight at ambient temperature. Following this step the mixture was centrifuged to remove the resin, and components of the polymerization mixture (solvent, monomers, initiator and adhesion promoter) were each carefully weighed and homogenized. The mixture was then immediately forced through the capillary where synthesis took place upon exposure to UV light. Preparation of a single batch took ~11 hours (including overnight removal of inhibitor and 1hr preparation), the time required and the highly reactive nature of the mixture could lead to column-to-column variability and was very costly in terms of preparation effort. Therefore a simplified, more streamlined process could be very beneficial since it would reduce variability due to manufacturing and decrease the overall column preparation time.

The approach was to prepare a stock solution of the polymerization mixture, that was aliquotted into smaller individual volumes and immediately frozen at -80C. Previous studies done by Cabral suggested that polymerization in the presence of the UV initiator did not occur under ambient conditions until the mix was exposed to UV light [54]. In order to further decrease the reactivity of the mixture, the inhibitors were not removed. The new method then entailed thawing individual aliquotes at room temperature, and homogenizing the mixture just prior to injection into the capillary. This new approach greatly reduced preparation time per column (10 minutes compared to 11 hours previously) and resulted in improved reproducibility. The solutions were tested over a period of 3 months and the column porosity variability was less than 4% (Table 3-2). The new approach was a significant improvement, both in terms of manufacture time and reproducibility, over the original method.

Table 3-2. Porosity reproducibility of column prepared at 20°C, exposed to UV for 20 min with m:p of 1:3. Prepared on 2 separate days separated by 7 days

	column-to-column (Batch 1)	**column-to-column (Batch 2)**	**batch-to-batch (Batch 1&2)**	**day-to-day (Batch 1)**
avg	0.70	0.70	0.70	0.73
std dev	0.01	0.01	0.01	0.03
n	3	5	8	3

3.2 Monolith characterization by SEM and AFM

The monoliths were imaged with SEM and AFM, and data from the particle size distribution was used to relate morphology to the monolith synthetic conditions (T, t, and m:p) and chromatographic behaviour.

3.2.1 AFM

AFM and SEM are complementary techniques for the study of surface and topography; however AFM provides much greater topographic resolution and direct height measurements of surface features. In addition, AFM allows the samples to be probed under wetted conditions that are similar to those used during chromatography. An AFM image of a 5µm × 10 µm area was collected in tapping mode in air and is presented in Figure 3-2. Analysis of the image with Nanoscope III v 7.30 software revealed the presence of large macro pores between 80 – 200 nm, however mesopores (2 – 50 nm) were not detected. The particles ranged in size from 0.4 – 1.5 µm, which was comparable to 0.6 – 0.9 μm range observed in SEM for the same sample and 0.3 – 2.0 μm reported by Cabral *et al.* for a similar sample in air [46].

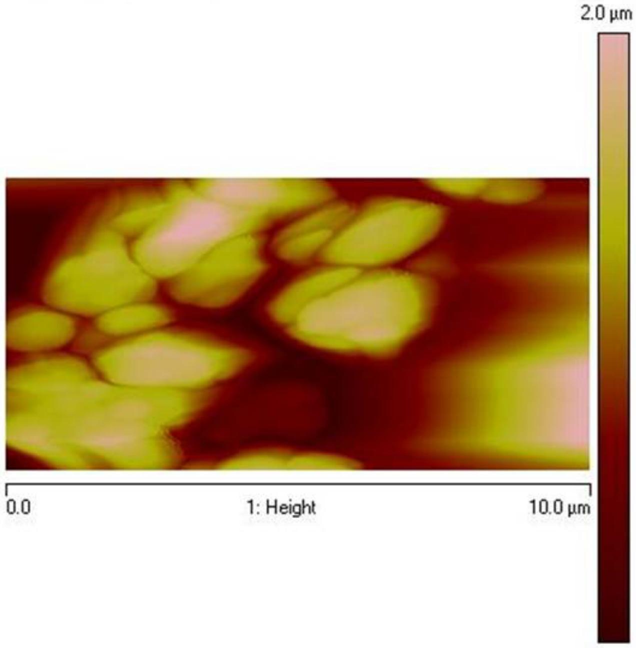

Figure 3-2. AFM image in air using tapping mode; the polymer was synthesized at 20°C, 20 min UV exposure time with 1:2 m:p mixture

In addition to the image of the polymer obtained in air, a different segment of the same capillary was imaged in water using tapping mode and is presented in Figure 3-3.

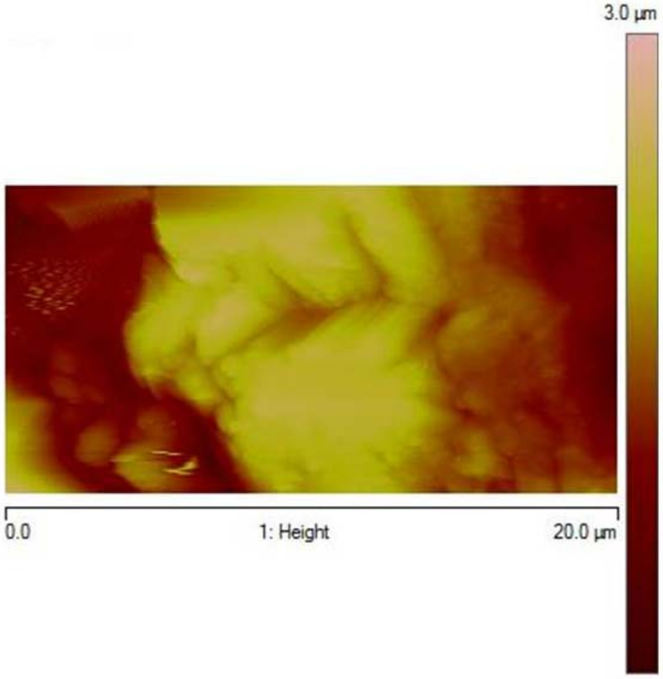

Figure 3-3. AFM image in water in tapping mode; polymer was synthesized with 1:2 m:p mixture at 20°C and 20 min UV exposure time

The analysis of the 20 µm × 10 µm section showed the presence of large through pores between 200 – 300 nm. The particles measured in water here (1.1 – 2.8 µm) were significantly larger than the particle dimensions obtained by Cabral *et al.* under the same conditions (0.2 – 1.5 µm) [46]. The pore sizes observed in the liquid medium were in the 150 – 200 nm range and pores below 50 nm were not detected. The findings are summarized in Table 3-3 below.

Table 3-3. Surface parameters determined by AFM (n=1)

	Air	**Water**
Particle Size (µm)	0.4-1.5	1.1-2.8
Through Pores (nm)	80-200	200-300
Image Surface Area (µm^2)	50	200
Root-mean-square roughness Rq* (nm)	140-260	106-150

*Rq: std dev of the surface in its height distributions

Multiple sections of the image which were representative of the surface of the monolith were analyzed with imaging software. Due to the non-homogeneous surface of the sample the root-mean-square roughness (Rq) showed considerable variability, however it was lower in water, which might be attributed to the polymer's expansion. The lack of mesopores (2 – 50 nm) on the surface of the globules was evident in both air and water.

It remains difficult to reach a definitive conclusion regarding the behaviour of the polymer in water because of insufficient data. Multiple images of the monolith must be obtained in order to gain better understanding of the natural variability in particle sizes and roughness, however only one image of sufficient resolution to provide meaningful data by AFM was collected. One significant problem with the analysis and imaging was the highly reticulated polymer surface. It proved to be very challenging to find a relatively flat region of 50 μm × 50 μm size. Hence smaller areas of 10 μm × 5 μm and 20 μm × 10 μm were imaged potentially introducing bias to the results.

In spite of these difficulties, AFM imaging remains the most effective way to gather information regarding pore sizes in the 30 – 50 nm range and can be a very useful tool in tandem with other techniques for the analysis of polymers under wetted conditions. In addition, chemical mapping is possible through the use of derivatized AFM tips, which would allow insight into the distribution of hydrophobic (butyl) and hydrophilic (sulfonate) functionalities.

3.2.2 SEM

3.2.2.1 Time and UV light intensity probed by SEM

In order to study the effect of exposure time on the progress of polymerization, a capillary was filled with a standard polymerization mix (m:p = 1:2, T = 20 ^{o}C) and placed under the UV lamp. Different segments of the capillary were exposed to UV light for periods of time ranging from 1 min to 40 mins. The capillary was flushed with ACN to remove unreacted monomers and imaged by SEM (See Figure 3-4).

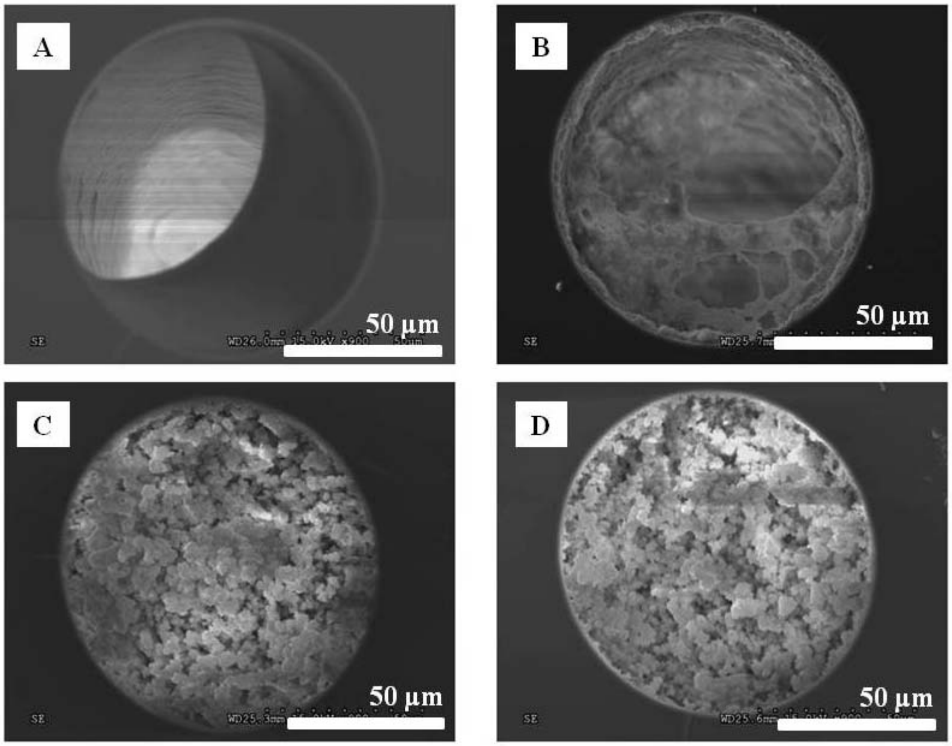

Figure 3-4. Polymerization time studies A)1 min exposure B) 2 min exposure C) 4 min exposure D) 8 min exposure

The time studies showed that 1 min was insufficient for polymerization but it was sufficient to form a thin layer of polymer at the wall surface (Figure 3-4-A). At 2 min the polymerization had started to progress from the wall towards the capillary interior and formed web-like structures (Figure 3-4-B). At this early stage the particles were quite small and not globular, and mainly the primary nuclei structure was seen. Within 4 minutes the interior of the capillary was filled with globules and this overall structure remained unchanged for the duration of the experiment (Figure 3-4-C). The polymerization possibly continued within the nuclei after 8 min but the globule size changes were minor and below the resolving power of SEM (See Appendix C).

In order to study the effect of UV light intensity, capillaries were filled with the standard polymerization mix (m:p = 1:2 at T = 20°C) and placed under a UV lamp for 10 min under different UV light intensities. The UV light intensity was controlled by placing fused silica metallic neutral density filters directly below the UV source. The filters' optical density (OD) ranged from 0.1 to 1.0 OD. Such filters are used to reduce the UV light intensity by a known factor. A filter with 1.0 OD will transmit only 10% of the initial UV light. In order to compensate for the lower UV light intensity exposure, the reaction time must be increased. For example, 1 min exposure under the initial UV light will be equivalent to 10 min exposure under the same light with 1.0 OD filter.

The UV light intensity has been related to the breakdown rate of the photoinitiator [55] and would be expected to affect the time needed to complete the reaction and possibly the structure of the polymer. The rate of primary nuclei formation is influenced by the UV light, while the growth of the nuclei into globules is controlled by exposure time. The effect of decreasing the UV light intensity to 10% (1.0 OD), 30% (0.5 OD), 50 % (0.3 OD) and 80% (0.1 OD) of its initial value was investigated by SEM.

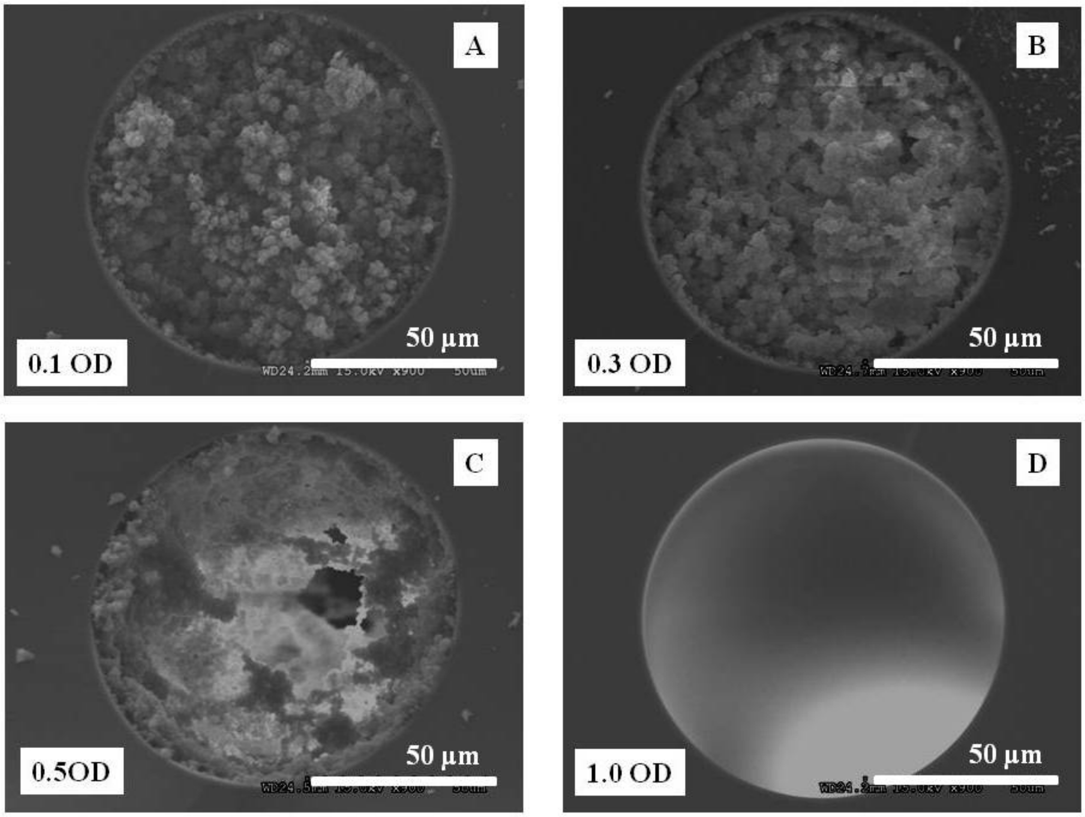

Figure 3-5. SEM images of polymer irradiated for 10 min under UV light that was filtered with fused silica metallic neutral density filters. UV light intensity output at 50 cm below the light source was 1.8 W/cm^2

A filter with 1.0 OD transmitted only 10% of the initial UV light and 10 min exposure time under these conditions was equivalent to 1 min exposure time under normal unfiltered UV light. As previously mentioned, 1 min was found to be insufficient to initiate the reaction and no polymerization was observed (Figure 3-5-A *vs.* Figure 3-4-A). In the same way, exposure under the 0.5 OD filter for 10 minutes was equivalent to 3 min exposure under normal light. As expected, the SEM image under these conditions was similar to the one obtained at 2 min in the time studies (Figure 3-5-B *vs.* Figure 3-4-B). The images of polymers made using 0.3 and 0.1 OD filters (equivalent to 5 and 8 min irradiation under normal light respectively) looked very similar to each other (Figure 3-17-C and Figure 3-5-D). This was expected because the previous time studies had shown that the majority of the polymer network was completed within 4 min under normal conditions (Figure 3-4). This is why the changes in structure were not readily detected by SEM.

The UV intensity studies showed that the size of the globules was not affected by the weakened UV light intensity, but they confirmed the relationship between UV light intensity and polymerization time. Even though the columns had similar macrostructure it is uncertain whether they have similar chromatographic behaviour. Further chromatographic studies must be performed to determine whether more subtle structural differences were present. These experiments demonstrate the importance of reporting UV light intensity during polymerization conditions. Differences in that parameter would lead to differences in the polymerization time required to complete the reaction.

3.2.2.2 Monolith characterization by SEM

All 27 columns used in the full 3^3 factorial design described in Section 3.3.2 were imaged by SEM. The images revealed a network of globules of relatively uniform size that were agglomerated in large clusters. A set of four images that showcase the monoliths with the biggest structural differences are presented in Figure 3-5 (the full set of 27 images is available in Appendix B). The particle dimensions were obtained by measuring the diameters across several particles ($n \geq 20$) and taking the average. The results presented in Table 3-4 demonstrated that the variety of T, t and m:p conditions produced polymers with a wide range of particle sizes and columns with identical porosities could still have dramatically different particle dimensions which would affect the chromatographic behaviour.

Table 3-4 SEM studies of particle size

T	t	m:p	Min (µm)	Max (µm)	Avg (µm)	Porosity
-1	-1	-1	0.4	0.9	0.7	0.61
-1	-1	0	0.5	0.7	0.6	0.73
-1	-1	1	0.3	0.5	0.4	0.75
-1	0	-1	0.8	1.0	0.9	0.67
-1	0	0	0.5	0.8	0.8	0.80
-1	0	1	0.4	0.6	0.6	0.85
-1	1	-1	0.5	0.9	**0.7***	0.67
-1	1	0	0.4	0.8	0.7	0.79
-1	1	1	0.3	0.5	0.4	0.88
0	-1	-1	0.7	0.9	0.8	0.66
0	-1	0	0.4	0.8	0.7	0.86
0	-1	1	0.4	0.8	**0.5***	0.90
0	0	-1	0.6	0.9	0.8	0.65
0	0	0	0.5	0.8	0.7	0.71
0	0	1	0.4	0.6	0.5	0.87
0	1	-1	0.6	0.8	0.7	0.70
0	1	0	0.4	0.6	0.5	0.77
0	1	1	0.4	0.7	0.5	0.88
1	-1	-1	0.5	0.8	0.7	0.65
1	-1	0	0.4	0.8	0.7	0.77
1	-1	1	0.4	0.7	0.5	0.86
1	0	-1	0.8	1.4	1.1	0.66
1	0	0	0.6	0.9	**0.7***	0.77
1	0	1	0.4	0.5	0.5	0.96
1	1	-1	0.5	1.2	1.1	0.60
1	1	0	0.5	0.9	**0.6***	0.71
1	1	1	0.5	0.7	0.6	0.76

***bimodal particle distribution**

Close inspection of the images revealed that the size of the microglobules was in the 0.4-1.1 µm range. There were four distinct groups of polymers: uniform with average globule size, uniform with large globules, uniform with small globules and polymers with bimodal size distribution of small and large globules. Nearly half of the imaged polymers showed uniform structure with an average globule size between 0.6 – 0.8 μm. Only four cases exhibited bimodal particle size distribution, where particles as small as 0.4 μm were evenly distributed among globules as large as 0.9 μm see Figure 3-5 D. In another 4 cases the polymer consisted primarily of small particles of about 0.4-0.5 μm. Only 3 columns had predominantly uniform large globules ranging from 0.9 to 1.1 μm. Non-uniformities in the particle size distribution would strongly affect all terms in the van Deemter equation (Equation 9). The A-term (Eddy diffusion-term) increases, because the difference in flowpaths for the analyte would increase for polydisperse particles [11]. The B-term (longitudinal diffusion) will also increase due to the non-uniform size of the packing because B is proportional to tortuosity and non-uniformities in the path lengths will increase the tortuosity term. The C-term (resistance to mass transfer) is also influenced by particle diameter. The proportion of the large particles will contribute towards the band broadening process. As particles get bigger, the spaces between them increase and diffusion of the analyte takes place over longer distances and becomes slower [11]. Therefore the presence of large particles and particle size non-uniformities will reduce the column efficiency.

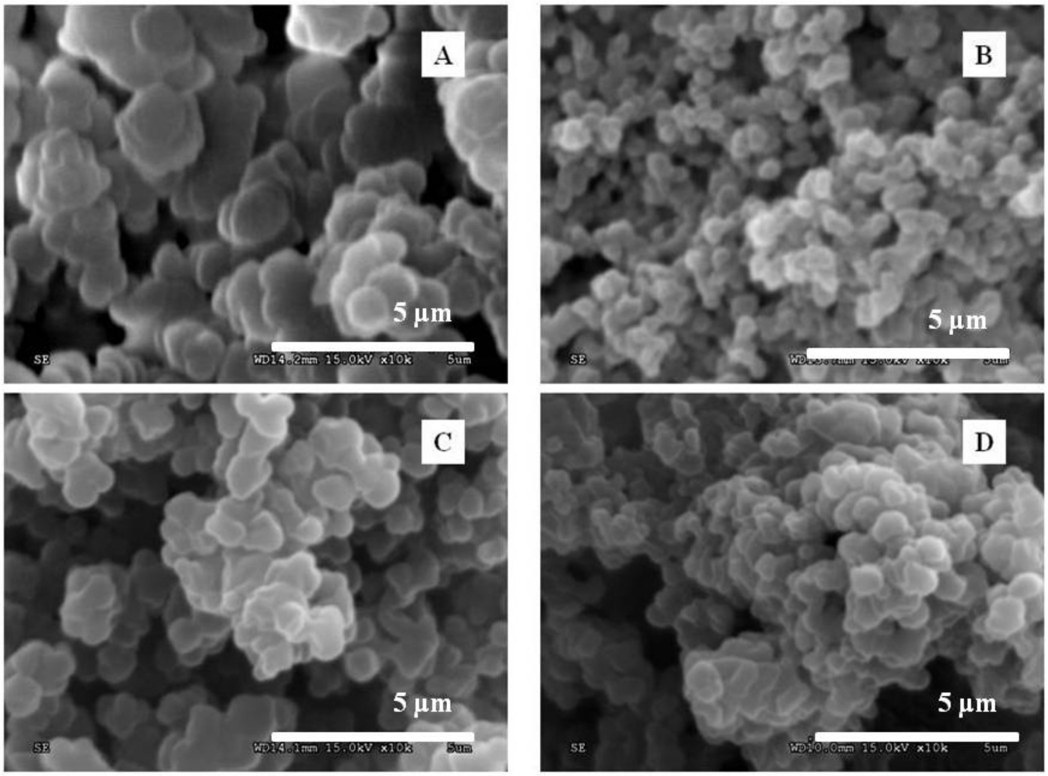

Figure 3-6. SEM images of four types of polymer structures found in the study; A) large particles B) small particles C) average size particles D) bimodal size distribution

It can be difficult to observe patterns in the structural changes since nearly half of all 27 columns exhibited similar structure and had uniformly distributed particles with size range of 0.6 – 0.8 µm. However, changes in monolith structure were successfully correlated to those regions in the experimental domain that were predicted to have maxima or minima in the porosity and k' by the factorial design models. For example, in the regions where porosity was predicted to be at its maximum but k' was at its minimum, the polymers consisted primarily of small globules (0.5 µm on avg.). These polymers were made with m:p of 1:4 which suggested that there was less stationary phase per unit volume and hence poorer chromatographic retention (Figure 3-5 B). As previously discussed, columns have an optimal stationary phase surface for chromatography when porosity was within 0.6 – 0.7. The columns that were predicted to have porosity within this target range and maximum k' also had the biggest particle sizes (around 1.0 μm, Figure 3-5 A). Columns with porosity within the target range have relatively low backpressure. The restriction of volumetric flow due to the presence of the packing, limits the ion flow velocity in a packed capillary and controls the EOF. Low back pressure is important since columns need to be flushed by pressure when solvents are changed or air bubbles are trapped within the column.

The T parameter was a significant variable in the models for porosity and k'. When the T×t was optimal in the porosity model and T and m:p were optimal in the k' model, the monolith had the highest retention and uniform globules of 0.7μm (Figure 3-15 C). It has been previously reported that T affects the pore size distribution and globule size [38]. Generally as T increased, the volume fraction of the smaller pores increased along with the monolith surface area. This was confirmed by the k' model since T increase was related to increase in retention. These findings suggested that T possibly affected the specific surface area and pore volume and could prove to be an important parameter in the development of stationary phases with target properties. The effect of T on the surface area can be explained by changes in the nucleation rate during polymerization. The rate of initiator decomposition increases at higher T leading to the formation of larger number of nuclei and globules; since the amount of monomers is constant, the higher nucleation rate leads to the formation of more globules, but of a smaller size; the large fraction of smaller interconnected globules leads to the formation of smaller voids and pores that increase the overall surface area. These results showed that SEM screening in combination with factorial design models could be a convenient tool for the rapid identification of suitable stationary phases for target chromatographic separations. Imaging techniques such as SEM and AFM can help investigate the relationship between the morphology of a monolith and its chromatographic behaviour, since the surface of the stationary phase greatly affects the separation process. However, an important limitation of some imaging techniques is that they are often carried out using dry monoliths, but under chromatographic conditions the monolith is solvated. Solvation plays an important role during the separation process, since it changes pore dimensions, thus the visualization of the dry monolith will not always accurately reflect the microglobular structure under chromatographic conditions.

3.3 Monolith characterization by factorial design

As already discussed the porosity is an important characterization parameter because it is a metric for the amount of stationary phase available for interaction with the analyte. Therefore, in principle, the porosity can be used as a reasonable predictor of the chromatographic behaviour of the column. Since the porosity is a function of many parameters (i.e. T, t, m:p, solvent type, monomer type, amount of cross linker, and amount of initiator) it was important to study the impact and significance of each of these factors not only individually, but also and in combination with others (i.e. interactive effects). While T, t, and m:p mainly impact the stationary phase morphology, the remaining variables impact the chemistry of the polymer [56]. Therefore initial efforts at studying this system were directed towards T, t and m:p because they significantly affected morphology without affecting the polymer chemistry, in addition to being easily controlled experimentally.

3.3.1 Validation of porosity measurements

The home built CEC system was used to measure the conductivity of small columns (5 cm and above) and it made it possible to compare whether conductivity measured by two methods (whole column vs. cut column) would result in equivalent porosity values.

Using the 'whole column' method the porosity was determined to be 0.64 ± 0.01, while cutting the column into two segments and measuring the conductivity of each yielded a porosity of 0.66 ± 0.01. The difference in porosity values measured by both methods was not significant at 95% confidence level as determined by a T-test. This showed that the non-destructive conductivity method using the entire column was an accurate method for determining porosity and was therefore used throughout the remainder of the thesis to measure porosity.

To test whether the conductivity of the open segment was influenced by the pre-treatment and silanization process the conductivity of several capillaries that had been treated with silanization mixture for different amounts of time was measured (Table 3-5).

Table 3-5. Impact of silanization time on conductivity of an open capillary measured at 8 kV with 50/50 5 mM borate pH 10/ACN buffer (% v/v), capillary I.D. 100 μm, L_{tot} = 20 cm.

silanization time (hrs)	σ open $\times 10^{-4}\ \Omega^{-1}\ cm^{-1}$	Std dev $\times 10^{-5}\Omega^{-1}\ cm^{-1}$	Rsd (%)
1	1.58	0.57	3.64
2	1.53	0.83	5.43
4	1.59	≈ 0	≈ 0.00
8	1.57	0.37	2.34
24	1.55	1.05	6.78
Avg	***1.56***		
Std dev	***0.03***		
% rsd	***1.63***		

***n = 3**

This experiment revealed that increasing the silanization time had no systematic effect on the conductivity of the open segment. This correlated with previous findings (Table 3-1) that the silanization reaction was rapid and completed within 1 hr. Multiple conductivity measurements were made on a pre-treated open capillaries (Table 3-6) and the average conductivity was used to calculate the conductivity ratio ϕ and the porosity ε throughout the thesis.

Table 3-6. Conductivity measurements of open silanized capillaries at 8 kV with (50/50) 5 mM borate pH 10/ACN buffer (% v/v), capillary I.D. 100 μm, length 30.5 cm

silanization time (hrs)	σ open$\times 10^{-4}$ $\Omega^{-1}\ cm^{-1}$
12	1.44
12	1.41
12	1.53
12	1.45
avg	***1.46***
Std dev	***0.05***

3.3.2 Chemometric study of monolith porosity

Multivariate data analysis was employed to probe for the presence of interactions between variables and the effect of variables on the porosity. This study employed a three-level, three-factor full factorial design that was used to generate a second degree polynomial model for the porosity of CEC columns. The three factors (T, t and m:p) were each considered at 3 levels (low, medium and high). The full factorial design can be visualized using the 3D representation in Figure 3-7.

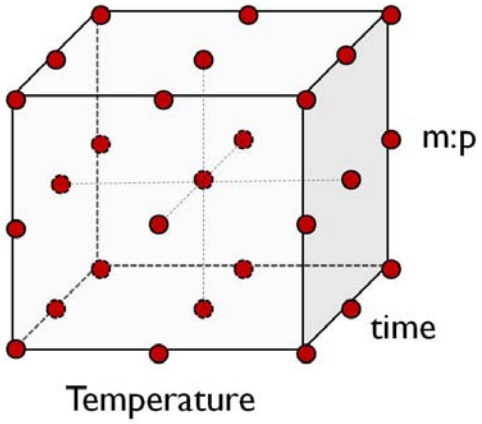

Figure 3-7. Graphical representation of 3^3 full factorial design

The temperature (T) range chosen was 0°C, 20°C and 40°C. It was convenient to perform experiments near room temperature because this did not require additional equipment. Temperature is known to affect reaction kinetics and typically the rate of the reaction doubles for every 10°C rise in temperature. Choosing reaction temperatures that were 20°C apart would be sufficient to observe changes in the porosity due to T. Furthermore, many of the components in the polymerization mixture were volatile and it was important to choose a range that was well below the boiling point and well above the freezing point of the mixture.

The SEM time studies (Section 3.2.2.1) revealed that the macroscopic structure of the polymer did not change after 8 min UV exposure at 20°C. At reaction times below 8 minutes the structure was incomplete and produced voids which would have a negative impact on the quality of the chromatography. The exposure times ranged between 10 and 30 min and were chosen to ensure that at high (and low) temperatures the time range would be sufficient to complete the polymer network.

The monomer to porogen (m:p) ratio is known to have the biggest impact, since the amount of porogen is proportional to the porosity. Excessively porous polymers ($\varepsilon > 0.8$) are not useful chromatographically because of their low stationary phase/mobile phase ratio and too packed polymers ($\varepsilon < 0.5$) are hard to flush due to high back pressure. Porosities of 0.6 – 0.7 are most desirable chromatographically. Initial experiments suggested that m:p ratios between 1:2 and 1:4 would meet the porosity needs.

The factorial design required the synthesis of 27 different CEC columns and 4 replicates according to Table 3-7 and Table 3-8.

Table 3-7. Manufacturing conditions for column preparations

	Levels		
Independent Variables	low (-1)	medium (0)	high (+1)
Temperature	0°C	20°C	40°C
time	10 min	20 min	30 min
m:p	1:2	1:3	1:4

Table 3-8. Variables and Levels according to 3^3 full factorial design

Factor 1 Temperature	Factor 2 time	Factor 3 m:p	Response Porosity
-1	-1	-1	0.61
-1	-1	0	0.73
-1	-1	1	0.75
-1	0	-1	0.67
-1	0	0	0.80
-1	0	1	0.85
-1	1	-1	0.67
-1	1	0	0.79
-1	1	1	0.88
0	-1	-1	0.66
0	-1	0	0.86
0	-1	1	0.90
0	0	-1	0.65
0	0	0	0.70
0	0	0	0.71
0	0	0	0.73
0	0	0	0.75
0	0	0	0.76
0	0	1	0.87
0	1	-1	0.70
0	1	0	0.77
0	1	1	0.88
1	-1	-1	0.65
1	-1	0	0.77
1	-1	1	0.86
1	0	-1	0.66
1	0	0	0.77
1	0	1	0.96
1	1	-1	0.60
1	1	0	0.71
1	1	1	0.76

The additional four true replicates were performed at 20°C, 20 min, 1:2, which corresponds to the central point of the experimental design (0,0,0). These replicates were done in order to provide adequate number of degrees of freedom for the calculation of model error estimates.

Typically only the center point in the design space is duplicated, however additional duplicates of other points can be performed, if better estimates of the porosity in those regions in the experimental space are needed. Replication increases the precision of the response estimate by averaging results, but more importantly, provides an independent estimate of the experimental variability over the design space. All columns were assessed for porosity using the methods outlined in Section 2.4. The columns had porosity values that ranged from 0.60 to 0.96 and different morphology and chromatographic behaviour, which are discussed in Section 3.2.2.2 and Section 3.3.3.

The results for the three-level three-factor full factorial design were validated in two ways: using analysis of variance (ANOVA) and testing against an additional validation data set. The model of the response surface of the porosity is presented in Figure 3-8.

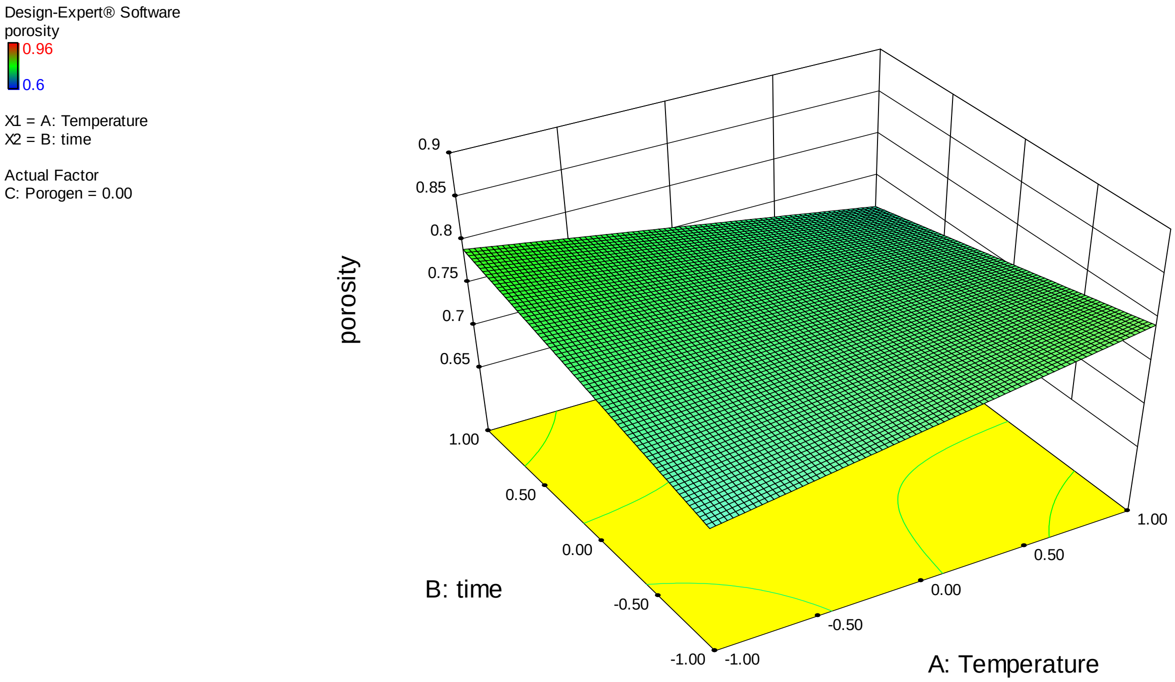

Figure 3-8. Porosity surface plot when m:p = 1:3

The p-value for the model was < 0.0001, which is substantially lower than the critical value of significance $p<0.05$ (at 95% confidence interval (CI)). The R^2 value for the model was 0.812, which means that 81.2% of the variance in the data can be explained by the model. A valid model should have a value of R^2 that is 0.60 or greater [57]. The predicted R^2 and the adjusted R^2 should be within 0.20 of each other otherwise there may be outliers or different type of models must be considered [58]. The predicted R^2 was 0.73 and it was in reasonable agreement with the adjusted R^2 of 0.78.

The adequate precision is a measure of the signal to noise ratio that compares the predicted values at the design points to the average prediction error; values greater than 4 indicate that the model can make adequate predictions [59]. For this model the adequate precision value was 16.52 and therefore the model was suitable for predicting porosity within the design space.

There are a number of diagnostic plots that help uncover underlying problems with the model. The normal probability plot is a diagnostic tool that is used to determine the distribution of the residuals. The residuals are related to the variation that is not explained by the model and are plotted in Figure 3-9 below. The normal probability plot tests the assumption that the variance of the data is normally distributed. If the data points are normally distributed about the straight line, then the normality assumption is justified. Small deviations from the straight line are common, however if the data is skewed the normality assumption is not justified**.**

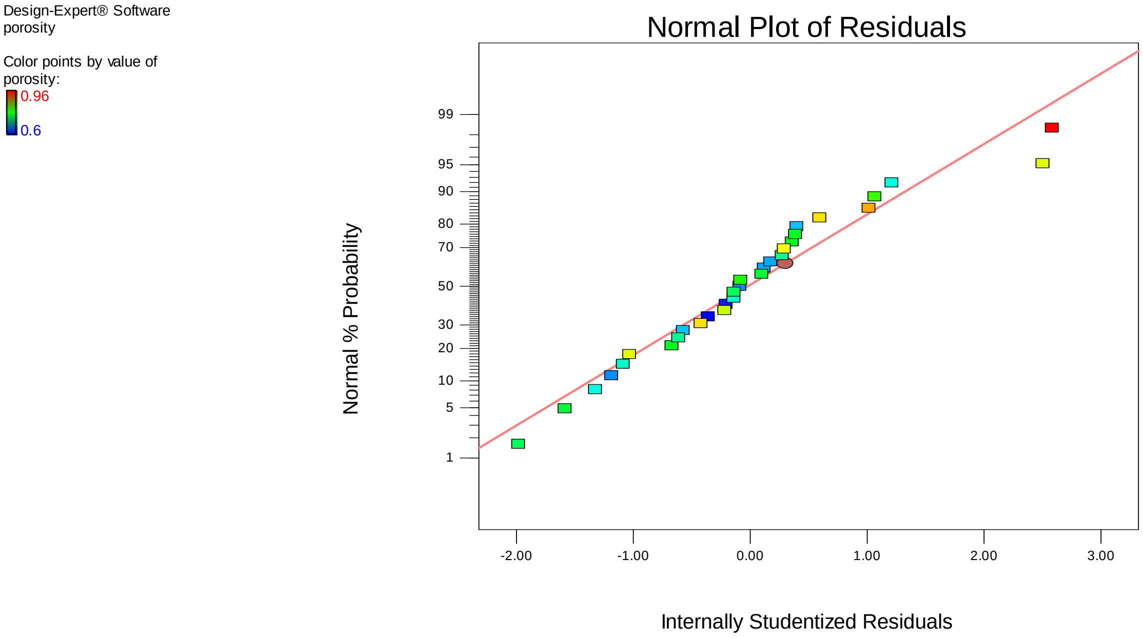

Figure 3-9. Normal probability plot

The normal probability plot revealed that the model had residuals that follow a normal distribution and as such the points fall onto a straight line, which indicated that the data was normally distributed and there was no systematic deviation between the model and the data and no additional transformation/normalization of the response data were necessary.

The predicted vs. actual plot is another diagnostic graph which helps visualize how well the model predicts the experimental outcome. If the predicted points match the actual points the data will follow a straight line. Typically some scatter is expected and the deviations should be normally distributed about the 1:1 line as shown in Figure 3-10**.**

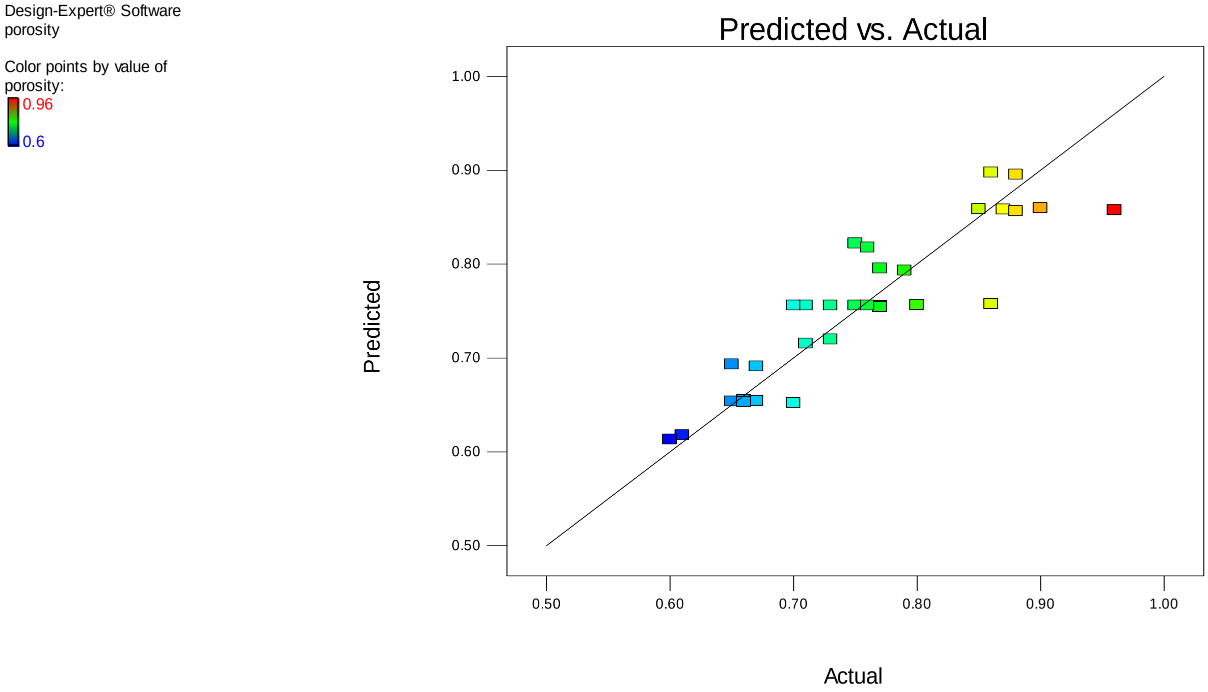

Figure 3-10 Predicted porosity vs. actual porosity plot

The R^2 value for a valid model is 0.6 or greater. For this model the R^2 was 0.81 indicating that model predictions would be accurate. The scatter was normally distributed about the 1:1 line and did not show systematic deviations or the presence of any outliers**.**

3.3.2.1 Validation of factorial design model

The ANOVA results from the model are summarized in Table 3-9.

Table 3-9 ANOVA for response surface using a two factor interaction reduced model

Source	Sum of Squares	Mean Square	F-Value	Probability $F_{obs} > F_{critical}$
Model	**0.206**	**0.051**	**27.996**	**< 0.0001***
T	<0.001	<0.001	0.003	0.957
t	<0.001	<0.001	0.027	0.870
m:p	**0.188**	**0.188**	**102.4**	**< 0.0001***
T×t	**0.018**	**0.018**	**9.596**	**0.005***
Lack of Fit	0.045	0.002	3.159	0.136
Pure Error	0.003	0.001	n/a	n/a

***significant < 0.05**

The model analysis suggested that m:p was a significant factor as was the T×t interaction. The T×m:p and t×m:p terms were not significant and were eliminated after backwards elimination regression. The T and t were not significant factors alone, but needed to be retained in the model in order to preserve hirarchy since their interaction term T×t was significant.

The lack of fit is a measure that compares the variation of the replicates about their mean values to the variation of the design points about their predicted values. It was calculated based on the four replicates of the central point in the design. The lack of fit F-value for the model was 3.159, which was greater than the critical F-value of 2.817. The probability that the observed F-value would be greater than the critical F-value due to noise was 0.136 (*i.e.* 13.6%), which at 95% confidence limit was not significant. The non-significant lack of fit was an indication that the model was a good fit for the data.

The mathematical relationship for the porosity as a function of T, t and m:p according to this model was represented in the form of a polynomial equation:

$$Porosity = 0.76 - 0.00056T - 0.0017t + 0.10m : p - 0.038T \times t$$

Equation 17. Porosity model based on full 3^3 factorial design

the confidence that this calibration equation would predict the observed values of porosity better than the mean for all porosity values was 95%.

The linear least squares analysis produced a result that was consistent with univariate analysis and chemical expectations, where porosity was proportional to the amount of porogen, this was reflected in the large positive coefficient of +0.10 for the m:p term, compared to the rest of the coefficients in the equation. This indicated that the m:p ratio had the biggest impact on porosity compared to the rest of the factors. The most interesting finding in this multivariate study was the interaction between T and t.

The interactive T×t term was statistically significant and had a high negative coefficient of - 0.038 in the model equation. This showed that the T×t term decreased the porosity whenever both T and t were low and both T and t were high, but porosity increased whenever T was low and t was high and vise versa. This relationship held true for any level of m:p within the experimental space (see Figure 3-11).

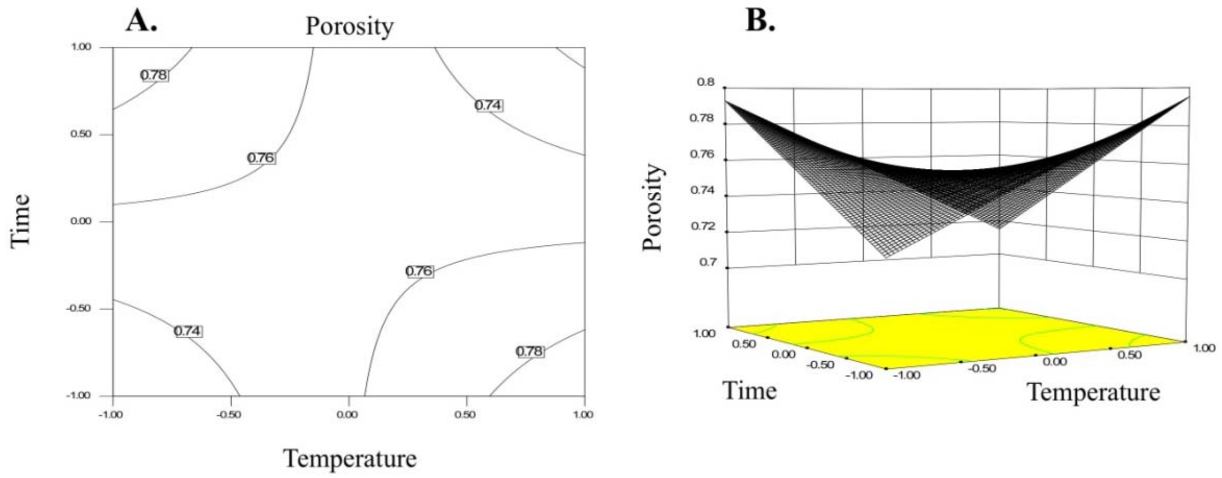

Figure 3-11. Contour plot (A) and 3D surface plot (B) showing the effects of T and t on porosity when m:p = 1:3

The contour plot showed that the differences in porosity were not drastic. This lead to the conclusion that the polymerization reaction completed the macro structure of the polymer relatively fast and minor (though still statistically significant) porosity differences of ± 0.04, were due to differences in the micro pore size.

The columns at the four corners of the contour plot in Figure 3-11 were imaged by SEM and are shown in Figure 3-12. The macrostructure of the polymers was somewhat similar, but there were slight differences in the globule size. The polymers with the slightly larger globules of 0.7μm had slightly higher porosity values of 0.78, which was likely due to the fact that there were slightly less globules per unit volume and the slightly bigger inter-particle spaces resulted in a more porous structure. However, the overall structural differences were subtle and were probably due to differences in the size and number of globules. This could be related to reaction kinetics because the breakdown rate of the reaction initiator controls the formation of primary nuclei and subsequent formation of secondary nuclei. The final particles are formed when the secondary nuclei combine with the primary nuclei.

As previously discussed in Section 1.5.1, there are two fronts of polymerization: within the primary nuclei and within the bulk solution (forming the secondary nuclei). At low T and short t (0°C, 10 min, respectively, porosity = 0.74 and particle size = 0.6 µm) the polymerization within the primary nuclei was kinetically preferred, however the short reaction time resulted in smaller sized uniform globules which were tightly packed and formed a dense polymer with low porosity. At high T and long t (40°C, 30 min, respectively, porosity = 0.74 and particle size = 0.5 – 0.9 µm), polymerization occurred on both fronts and there was bimodal size distribution of globules that ranged from 0.5 to 0.9 µm. The large particles formed by the coalescence of the primary and secondary nuclei made the polymer denser because the secondary nuclei filled in the spaces between the large particles resulting in a tightly packed structure with low porosity.

At high T and short t (40°C, 10 min) the polymerization continued on both fronts, however there was not enough time for the secondary nuclei to grow and coalesce, leading to the formation of mostly large, loosely packed globules and a more porous polymer structure (porosity = 0.78 and particle size = 0.7 µm). At low T and long t (0°C, 30 min) the polymerization occured mainly within the primary nuclei, which grew with time and a uniform, loosely packed, high porosity polymer is formed (porosity = 0.78 and particle size = 0.7 µm).

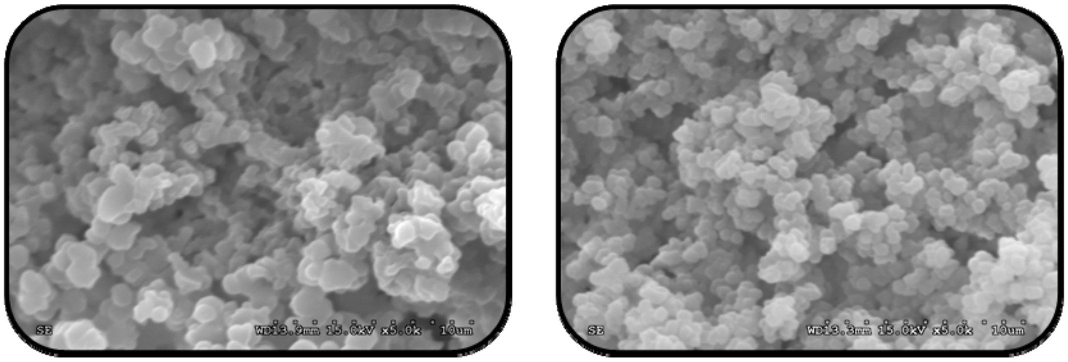

T = 40°C; t = 30 min
Porosity = 0.74;
size = 0.5 - 0.9 µm (bimodal)

T = 0°C; t = 30 min
Porosity = 0.78;
size = 0.7µm

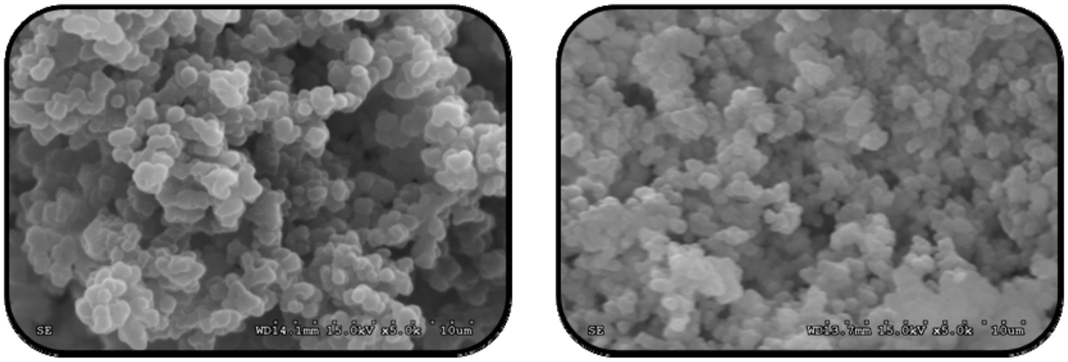

T = 40°C; t = 10 min
Porosity = 0.78;
size = 0.7µm

T = 0°C; t = 10 min
Porosity = 0.74;
size = 0.6µm

Figure 3-12. SEM images at 5K magnification; all capillaries were prepared with m:p = 1:3

In order to further validate the model an additional set of 15 CEC columns were made according to a reduced 3^3 factorial design model. The model was rebuilt with a smaller set of new samples in order to test if the same variables would be identified as significant. The new reduced 3^3 factorial design model is shown below.

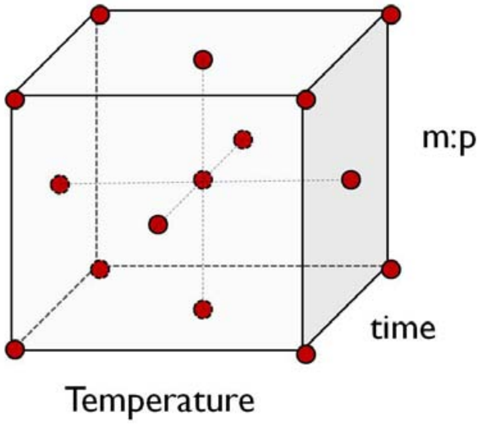

Figure 3-13. Reduced 3^3 factorial design model

The resulting matrix is presented in Table 3-10. The new values for porosity were in good agreement with the previous full 3^3 factorial design model and were on average within 4% of the porosities obtained before.

Table 3-10. Reduced 3^3 factorial design model porosity results

T	t	m:p	porosity
-1	-1	-1	0.59
-1	-1	1	0.73
-1	0	0	0.82
-1	1	-1	0.66
-1	1	1	0.87
0	-1	0	0.82
0	0	-1	0.61
0	0	0	0.73
0	0	1	0.81
0	1	0	0.76
1	-1	-1	0.71
1	-1	1	0.86
1	0	0	0.72
1	1	-1	0.56
1	1	1	0.71

The ANOVA of the data revealed that the model was significant at 95% CI and m:p was again determined to be the most significant factor followed by T×t (See Table 3-11).

Table 3-11. ANOVA of reduced 3^3 model

Source	Sum of Squares	Mean Square	F Value	Probability $F_{obs} > F_{critical}$
Model	**0.108**	**0.027**	**13.22**	**0.001***
T	0.001	0.001	0.59	0.460
t	0.002	0.002	1.10	0.319
m:p	**0.072**	**0.072**	**35.29**	**0.0001***
T×t	**0.033**	**0.033**	**15.88**	**0.003***
Residual	0.020	0.002		
Cor Total	0.129			

***significant < 0.05**

These results were in agreement with the full factorial model suggesting that reduced factorial design could be successfully used for studying this system. The full factorial design is a more robust method and will give more accurate predictions, however it identified only one major factor (m:p) and one significant two-factor interaction (T×t). Therefore, for this system the reduced factorial design would have enough capacity to distinguish the most important parameters while using a fraction of the data points. The reduced model was used in the following chromatography studies Section 3.3.3.

The reduced model yielded a second degree polynomial for the porosity where

$$Porosity = 0.73 - 0.011T - 0.015t + 0.085m : p - 0.064T \times t$$

Equation 18. Porosity model based on reduced 3^3 factorial design

Even though the equation was slightly different from that obtained with full 3^3 factorial design, the coefficients of the most significant terms m:p and T×t were similar and carry the same sign as expected. This demonstrated that both models identified the same factors as significant and confirmed that the reduced model was a faster and more efficient way of investigating the design space.

3.3.3 Chromatographic characterization of monoliths

The reduced 3^3 factorial design was used to study the chromatographic behaviour of the 15 columns described in the previous section. A CEC separation was performed in 20/80 (%v/v) mix of 5 mM borate, pH 10 and ACN buffer with three PAH's (Acenaphtene, Fluoranthene and Pyrene) and thiourea (non-retained marker). The chromatographic separation of PAH's was not based on differences in electrophoretic migration because the analytes were not charged, and therefore the separation mechanism was purely reverse phase. This was useful because it allowed to test the effect of T, t and m:p on the partitioning of PAH's between the stationary and the mobile phases.

Separations of the PAH mix were performed in triplicate on each of the 15 columns and the average relative standard deviation for the capacity factor (k') was less than 1.5%. The results are presented in Table 3-12.

Table 3-12. Reduced 3^3 factorial design k' results for acenaphene, fluoranthene, pyrene

Run	T	t	m:p	$k'_{Acenaphtene}$	$k'_{Fluoranthene}$	k'_{Pyrene}
1	-1	-1	-1	0.9	1.5	1.7
2	-1	-1	1	1.2	1.9	2.2
3	-1	0	0	1.1	1.7	2.0
4	-1	1	-1	0.9	1.5	1.7
5	-1	1	1	0.9	1.4	1.6
6	0	-1	0	1.0	1.6	1.9
7	0	0	-1	1.7	2.6	3.1
8	0	0	0	1.1	1.8	2.1
9	0	0	1	1.1	1.8	2.1
10	0	1	0	1.1	1.8	2.0
11	1	-1	-1	1.9	3.1	3.6
12	1	-1	1	0.9	1.4	1.6
13	1	0	0	1.2	2.0	2.3
14*	**1**	**1**	**-1**	**1.1**	**1.8**	**2.1**
15	1	1	1	0.9	1.4	1.6

***outlier**

The data analysis was performed with Design Expert V8 software using a two-factor interaction model. After building the model, a careful inspection of influence plots revealed that there was an outlier. Influence plots assist in determining whether individual points have undue impact on the fitted regression model, and can be a justification for the removal of outliers.

The externally Studentized residuals plot is an influence plot that shows the standard deviation of the actual value compared to the standard deviation of the predicted value when the model is built without the point in question (Figure 3-14). Points that are outside the significance threshold limit at 95% CI are potential outliers and the model could be justifiably improved by removing such points from the design.

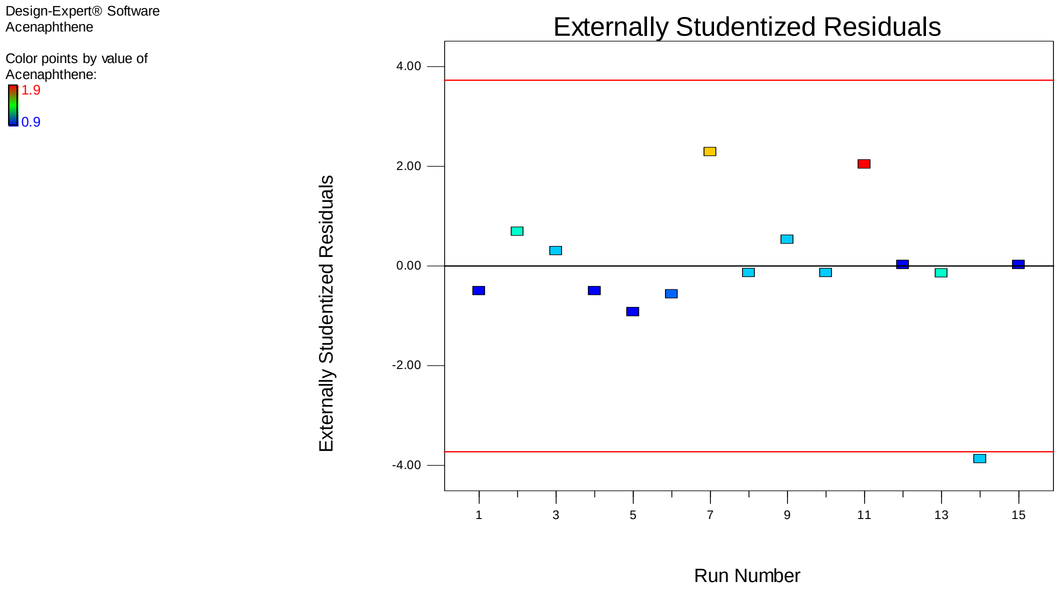

Figure 3-14. Externally studentized residuals plot; 95% CI limits cut off line (in red)

The plot in Figure 3-14 revealed that run 14 was a potential outlier. This was confirmed by an additional diagnostics plot of the Cook’s distance (Figure 3-15). The Cook's distance is used to quantify the influence of a point on the model, by the change in regression coefficients that occurs when the point in question is left out of the training set. Data points with large residuals and/or leverage can be identified as outliers in the Cook’s distance plot.

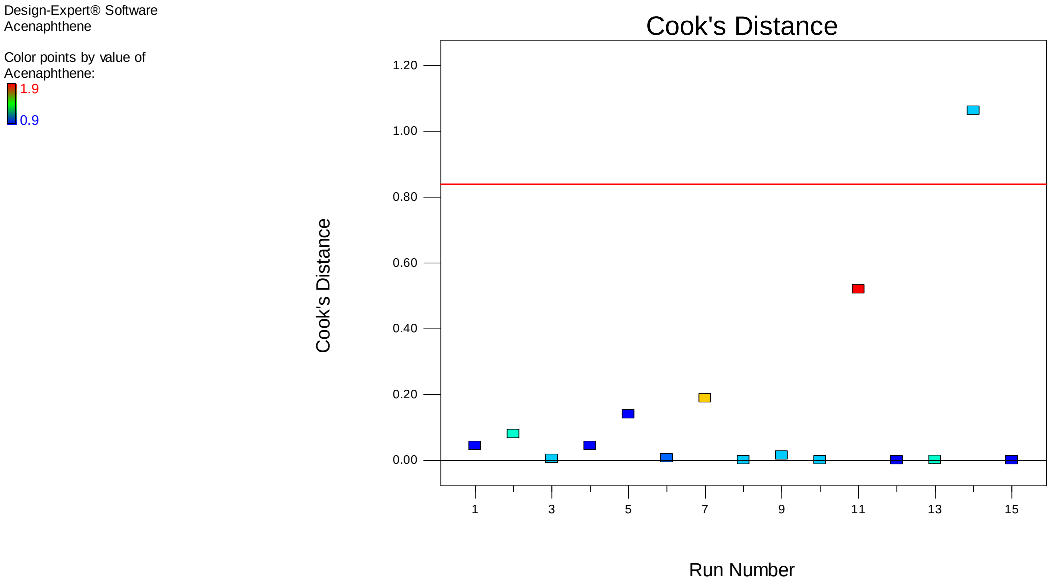

Figure 3-15. Cooks distance plot with all 15 points; in red 95% CI cut off line

This additional diagnostic plot also identified Run 14 as a potential outlier (see Figure 3-15). The point was well outside the 95% CI and it had an unduly high influence on the model. Once the point was removed from the model, the Cook's distance for the remaining points were well within the 95% CI (see Figure 3-16).

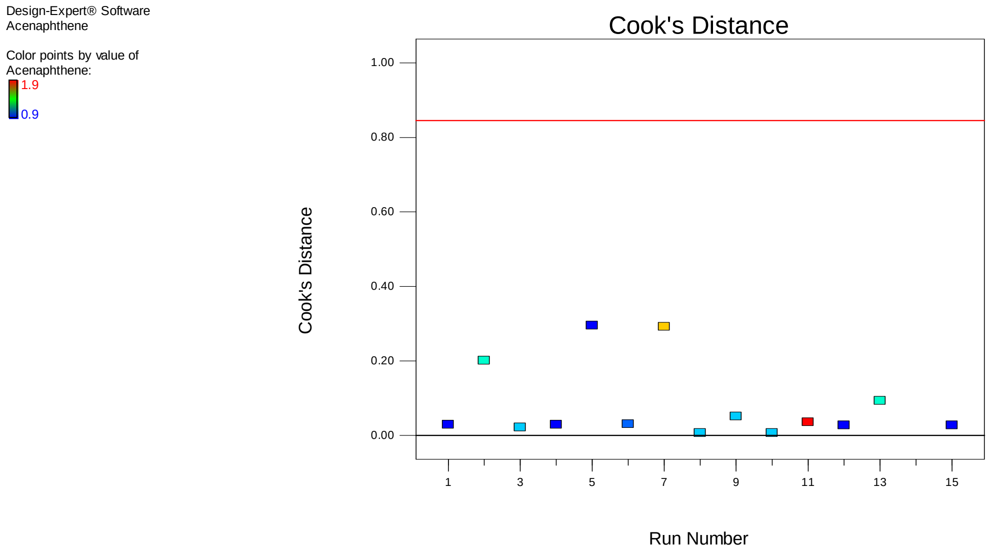

Figure 3-16. Cook’s distance after removing Run 14

The model was rebuilt with the remaining 14 points and the results suggested that the k’ for each PAH could be predicted based on T, t and m:p. The model identified T and m:p and T×m:p as statistically significant parameters that affected chromatographic performance of the monolith. The model suggested that the highest retention would be achieved at the highest T and the lowest m:p (T = 40°C, m:p = 1:2). This corresponded to the polymer with the highest surface area that had particles ranging from 0.5 - 0.8 µm with most particles of size 0.7µm (see Figure 3-17). The butyl monomer chain governed the hydrophobicity of the column, while the ratio of the porogenic solvent controlled porosity and separation efficiency.

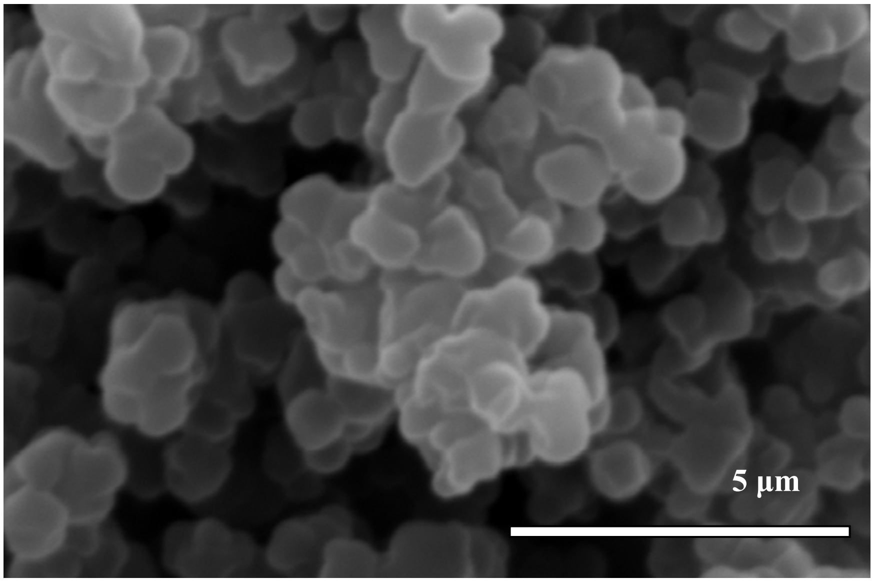

Figure 3-17. SEM image of polymer synthesized at 40°C, 10 min, m:p = 1:2 at 10K magnification

The column with the highest retention also correlated to the highest amount of monomer level tested in this study (m:p = 1:2). The SEM image revealed uniform particle structure or relatively small size. The column was synthesized at the minimum t (10 min) which was likely not sufficient to generate large secondary nuclei and the stationary phase consisted mostly of 0.7 µm uniform globules. This particle size was at the low range for columns that were made using m:p = 1:2. Surface area is inversely proportional to particle size, therefore this column had higher stationary phase surface area compared to other columns made using m:p = 1:2. The increased retention of this column was the result of the higher surface area of this stationary phase experienced by the analyte.

The k' model revealed that the most significant factors that impacted k' were T and m:p and their interaction T×m:p. In the porosity model m:p was also a significant factor, however T was only significant as a part of the T×t interaction. Both models show that T and m:p are important parameters that impact the structure and chromatographic behaviour of the monolith. These results suggested that porosity was not directly related to retention and could not be used to predict the chromatographic behaviour of the column, because retention and porosity are influenced by different set of factors.

The k' model generated equations for each PAH where k' was expressed a function of all significant parameters (SeeTable 3-13).

Table 3-13 Model for k' using reduced 3^3 factorial design

PAH	Model equation
Acenaphene	$k' = 1.18 + 0.18T - 0.23m{:}p - 0.28T \times m{:}p$
Fluoranthene	$k' = 1.90 + 0.29T - 0.38m{:}p - 0.45T \times m{:}p$
Pyrene	$k' = 2.20 + 0.34T - 0.45m{:}p - 0.54T \times m{:}p$

In all 3 cases the ANOVA test showed that the model was significant with a p-value of 0.001 or less (p-value of 0.05 or less was considered statistically significant at 95% CI). The R^2 for the models were between 0.80 – 0.84, and R^2 greater than 0.6 was considered statistically significant. The diagnostic plots described above (externally Studentized residuals plot, Cook's distance plot) performed on the data did not reveal the presence of outliers.

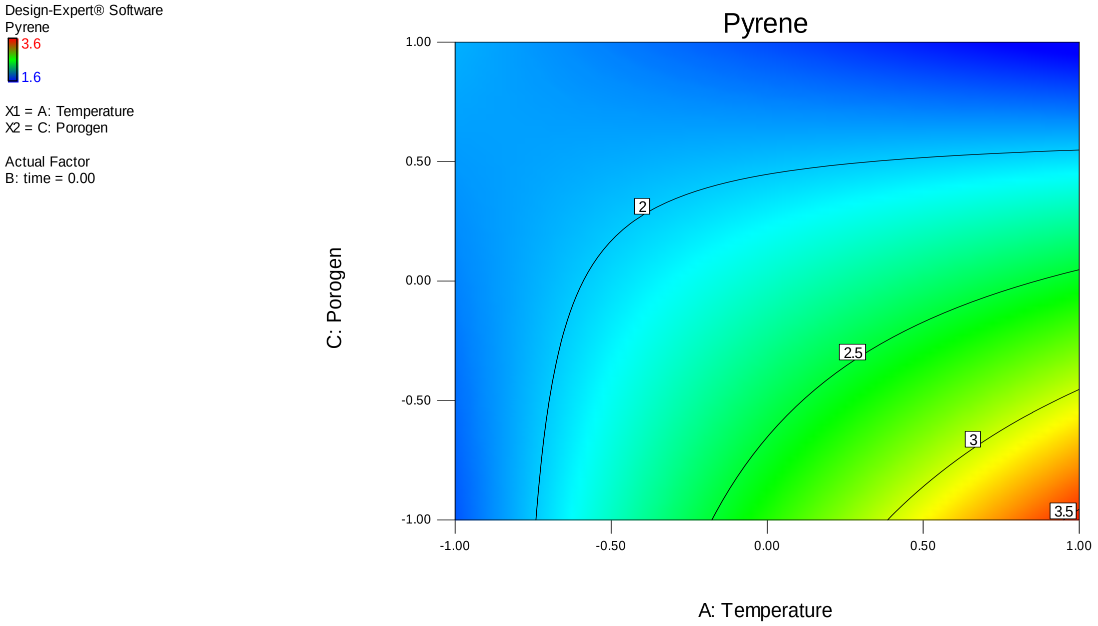

Figure 3-18. Contour plot of k' for pyrene

For all three PAH's the contour plots revealed that that the maximum k' values were in the region of lowest m:p and highest T (see Figure 3-18). This corresponded to a cube vertex in the 3D surface plot and in order to better investigate this relationship, the T and m:p ranges studied must be expanded, since the model is most accurate within the central region of the design space due to the higher number of points present.

The following Figure 3-19 shows a typical electrochromatogram for an injection of three PAH's with a mobile phase ACN – 5 mM borate, pH 10 80-20 (%v/v). The figure shows separations of the same sample on the columns with the highest (red) and lowest (black) retention coefficients.

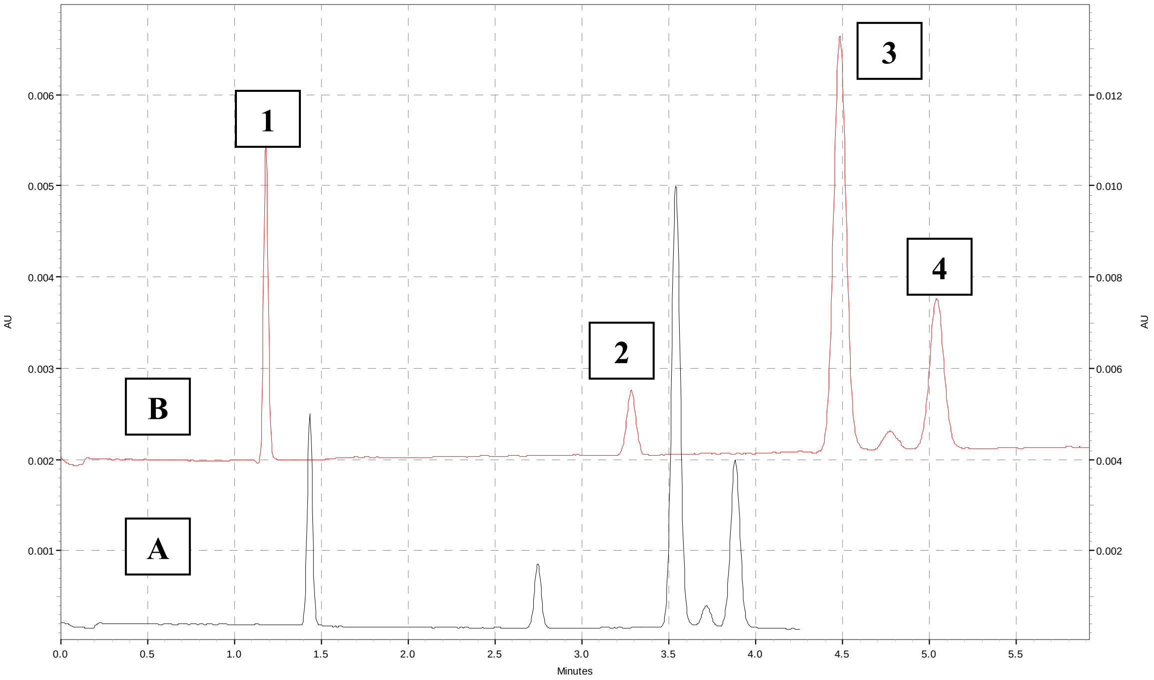

Figure 3-19. Separation of three PAHs and thiourea (**A**) column synthesized at 0°C, 10 min, m:p = 1:2 and (**B**) column synthesized at 20°C/20 min/m:p = 1:2; mobile phase – ACN/5mM borate, pH 10 80/20 (%v/v); separation voltage 8 kV; injection 2 sec at 5 kV. Order of elution Thiourea(1), Acenaphene (2), Fluoranthene (3), Pyrene (4);

The change in polymerization conditions affected the porosity, particle size and surface area of the monoliths and thus influenced column retention. The successful application of chemometrics to this complex system revealed that the retention behaviour could be modeled based on manufacturing conditions. This highlights the potential importance of the approach as it could aid in the selection of column manufacturing conditions that are targeted to a specific analyte (*e.g.* peptides, proteins, pesticides etc.). Even though the method would likely benefit from expanding the T and m:p ranges, further studies and rigorous testing of its predictive capabilities are needed. This approach could be a promising step towards controlling column properties in a very efficient manner.

3.4 Application to protein separations

Proteomics is pivotal to understanding biological systems and forms the framework of much clinical and pharmaceutical science [60-61]. Since proteins are incredibly diverse in their physicochemical nature (*e.g.*, hydrophobicity, size, isoelectric point, *etc.*) their analytical separation is a complex task. As a result, there has been increasing demand for the development of more efficient, faster, and simpler analytical tools. High efficiency CEC protein separations have been achieved using the poly(BAC-co-BDDA-co-AMPS) monolithic columns [54, 62-63]. This stationary phase has a dual chromatographic nature because it contains butyl groups (C4 functionality) as well as AMPS (sulfonate groups) and can provide reverse-phase combined with ion-exchange chromatography; in addition to these two mechanisms, the electrophoresis will also impact the final chromatographic separation as demonstrated with three model proteins by Bandilla *et al.* [64]. The pore diameter of the stationary phase is also an important parameter that influences the protein separations. The pores must be large enough to allow access to the stationary phase and generally 30 nm size pores are used in reverse phase protein separations.

In order to evaluate the potential of this monolith for the analysis of real biological samples, three major proteins that are commonly present in bovine milk were used as model proteins: α-lactalbumin, β-casein, and κ-casein (Table 3-14). These proteins were similar in molecular weight and pI values and thus preclude the size-exclusion separation mechanism as well as ion-exchange mechanism. The study of bovine milk samples could be used to develop diagnostic methods for testing milk quality; it can be valuable in monitoring udder health and identifying risk factors before the onset of infection.

Table 3-14 Milk protein properties

Protein	Number of Amino Acids	Molecular weight (Da)	GRAVY*	pI
α-lactalbumin	141	16133	-0.169	4.9
β-casein	224	25107	-0.154	5.3
κ-casein	190	21269	-0.287	6.3

*GRAVY (*grand average of hydropathy*); most hydrophilic (lowest negative), most hydrophobic (highest positive)

A mix of the three milk proteins and a neutral marker (thiourea) was separated in an open capillary in CE mode and it revealed that the proteins could not be baseline resolved using CE alone (Figure 3-20 Figure 3-21). The separation mechanism in CE was based on differences in the electric charge and hydrodynamic volume and the elution order was β-casein, α-lactalbumin followed by κ-casein. The proteins have relatively similar sizes and pI's and thus had similar electrophoretic mobility, hence their poor resolution in CE.

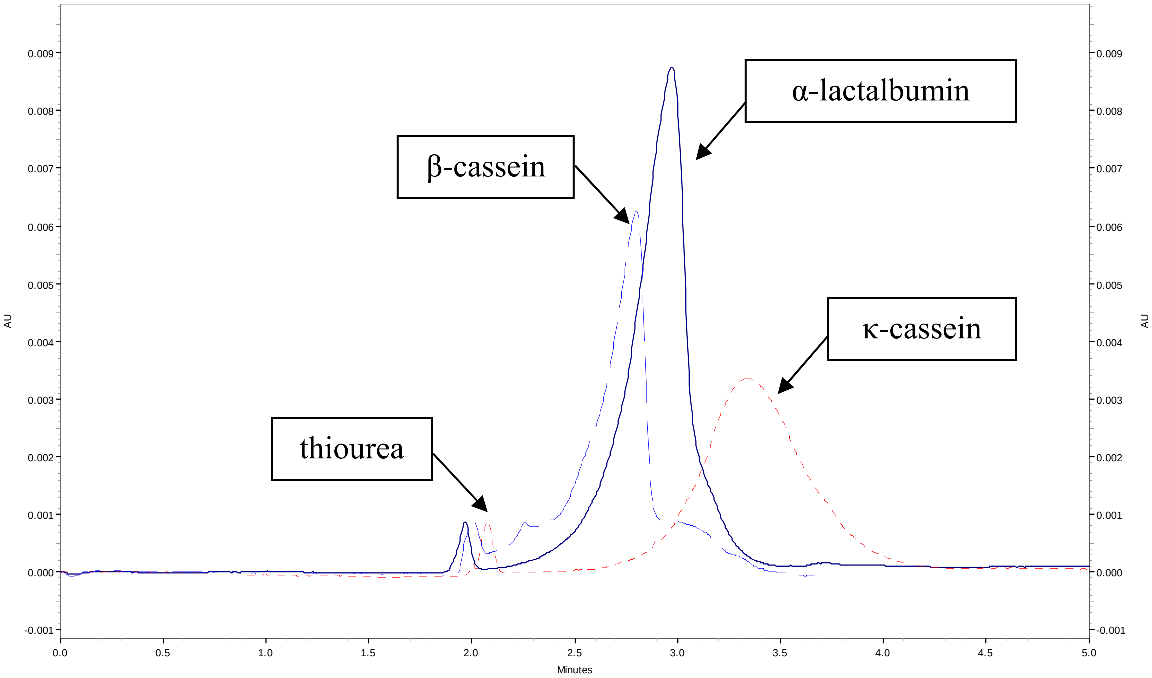

Figure 3-20. Overlaid electropherograms of thiourea and β-cassein (dashed line); thiourea and α-lactalbumin (solid line); thiourea and κ-cassein (dotted line); mobile phase: 50/50 (%v/v) 5 mM borate pH 10 /ACN buffer; separation voltage: 10 kV; injection 2 sec at 5 kV. L_{tot} = 30.5 cm L_{det} = 20.0 cm

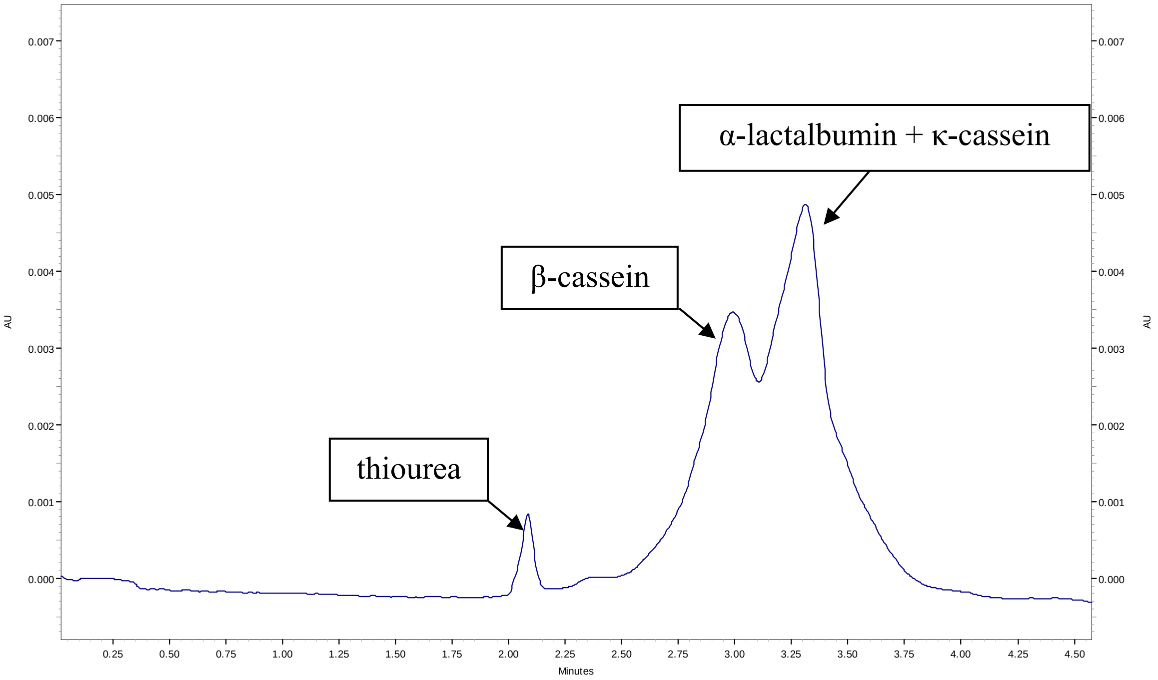

Figure 3-21. Electropherogram of model milk protein mixture: (1) thiourea (2) β-cassein and (3) α-lactalbumin + κ-cassein; mobile phase: 50/50 (%v/v) 5mM borate ph 10 /ACN buffer; separation voltage: 10 kV; injection: 2 sec at 5 kV. L_{tot} = 30.5 cm L_{det} = 20.0 cm

The protein separations were performed in CEC mode on monolithic columns that were synthesized at various conditions to test for effect on chromatography. Six columns were investigated and it became apparent that none of the columns were suitable for the separation of the model proteins, as baseline resolution of the model proteins was not achieved (Table 3-15, Figure 3-22).

Table 3-15. Resolution of model milk proteins

T	**t**	**m:p**	**k'** **α-lactalbumin**	**k'** **β-casein**	**k'** **κ-casein**	**porosity**
0	-1	0	1.3	0.7	0.8	0.82
0	0	-1	1.1	0.6	0.7	0.61
0	0	0	1.1	0.6	0.8	0.73
0	0	1	1.1	0.6	0.7	0.81
0	1	0	1.1	0.6	0.6	0.76
-1	-1	0	1.0	0.7	0.8	0.73
1	-1	-1	0.9	0.6	0.7	0.65

The CEC separation of the model proteins revealed the same elution order as previously investigated by Marie-Eve Beaudoin, namely β-casein, κ-casein followed by α-lactalbumin. However, in the current work the peaks were broad (10 – 30 sec at ½ height) and the plate number was very low (800 – 6000 N/m) and no baseline resolution was achieved. The different elution order compared to CE mode showed that the separation mechanism was not purely electrophoretic and there were different mechanisms at play.

The fixed sulfonate charges that were introduced in the stationary phase to support EOF may not be suitable for the separation of most proteins since they could introduce electrostatic interactions which could lead to band broadening and in some cases adsorption of the analytes [65]. In an effort to test the effect of AMPS on the protein separation, four columns with different % AMPS were prepared (Figure 3-22). The separation did not improve and the EOF mobility decreased with decreasing % AMPS as indicated by the elution time of the non-retained marker.

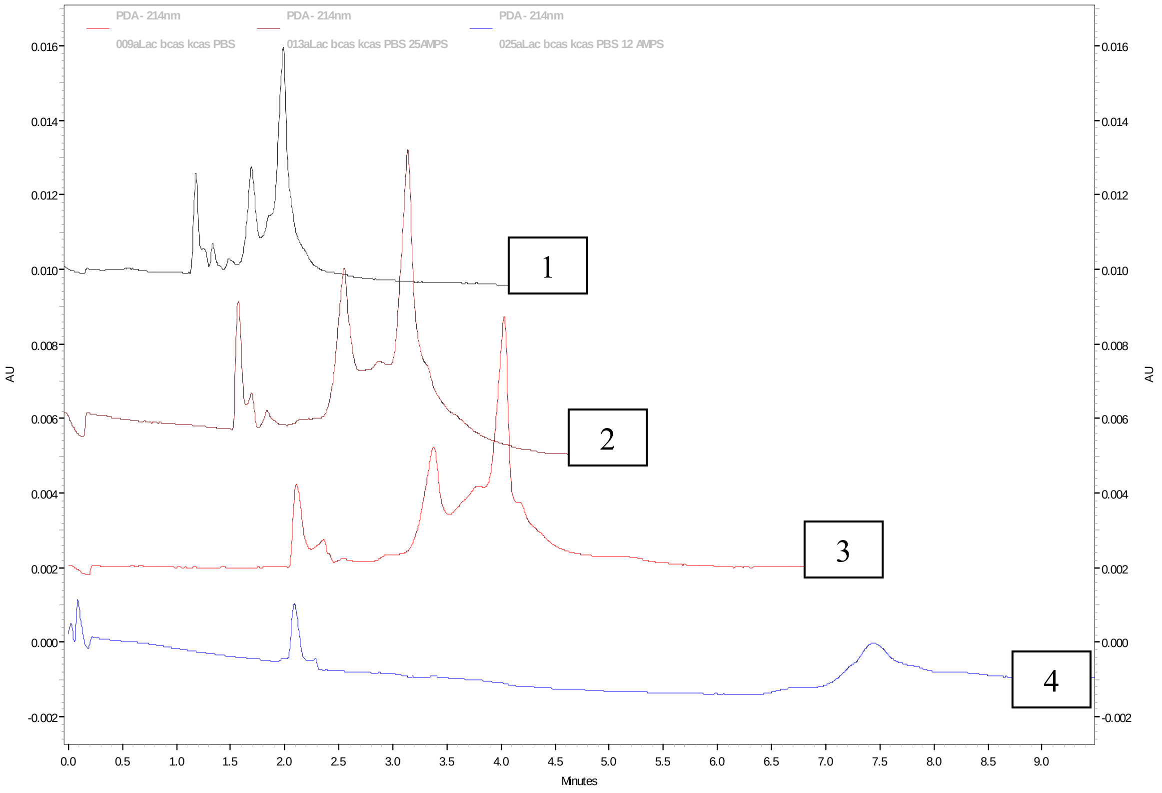

Figure 3-22. (1) 100% AMPS ; **(2)** 50% AMPS; **(3)** 25% AMPS ; **(4)** 12.5 % AMPS

The poor resolution in CEC was not surprising, given the low quality of the CE separation. The broad peaks in CE indicated that the proteins had high polydispersivity, which could explain the low efficiency of the CEC separation. The CEC separation mechanism was different than the CE mechanism, which was evident by the elution order of the analytes. In CEC the separation mechanism is governed by the presence of butyl groups (reverse phase) and sulfonate groups (negative charges). As % AMPS decreased, the sulfonate charges in the stationary phase also decreased leading to lower EOF. However, the EOF did not change significantly below 25% AMPS, possibly due to residual silanol groups on the capillary wall that were able to generate the EOF. The retention of the proteins increased as % AMPS decreased because the negative sulfonate charges repelled the negative charges on the proteins and as % AMPS decreased, the proteins interacted more strongly with the butyl groups on the stationary phase.

Chapter 4 Conclusions and Future Work

In this thesis, a novel streamlined manufacturing process to prepare monolithic capillaries for capillary electrochromatography was presented and characterized using factorial design. A comprehensive model was built, that can relate multiple synthetic conditions (i.e., temperature (T), monomer:porogen ratio (m:p), and time (t)) to relevant functional variables (i.e. porosity and column retention). To the best of my knowledge this is the first time that retention was modeled as a function of synthetic conditions using factorial design. This approach had the added benefits of reducing the total number of experiments needed and it helped reveal interactions between variables in ways that the one variable at a time approach was not capable of. Electrical measurements of the column conductivity were used to determine porosity, and a model relating porosity to synthetic conditions (i.e., T, m:p, and t) was built. The porosity model revealed that the amount of porogen had, as expected, a big impact on porosity and it identified a hereto unknown relationship between the t and T variables. The monolith chromatographic retention was characterized with a set of three PAHs, demonstrating its ability to separate neutral compounds based on purely reversed-phase chromatography. The chromatographic studies showed that columns synthesized under different conditions resulted in different retention factors (k') for the PAH's, and a model of k' as a function of T, t and m:p was built. The interactive T×m:p term was most significant with respect to retention, followed by the individual m:p and T terms. Both of these models suggest that T is an important factor that can be used to tailor the chromatographic character of the monolith. Inter- and intra-capillary reproducibility of less than 4%, with regards to porosity, indicated a reproducible manufacturing process.

The columns were applied to the separation of three model milk proteins, however the columns proved unsuitable to this application. It is likely the C4 group is not a suitable hydrophobic functionality for the separation of proteins. Future work should attempt to investigate and optimize the separation conditions and test additional model analytes. The chromatographic contribution could possibly be improved if a monolithic stationary phase with longer alkyl chains (e.g., C8) is used. If the poor interaction between the model proteins and stationary phase is mainly due to lack of pores in the 30 nm range, then investigating polymerization conditions with respect to pore size distribution can be another option. In this case the factorial design system would be a great benefit and a model should be built using retention (and possibly separation efficiency) as a function polymerization conditions.

Imaging by SEM revealed that polymerization inside a small capillary was directional, starting from the walls towards the center of the capillary. It is believed that this is the first report that the polymer is built along spindle-like structures. Preliminary AFM images showed that the polymer did not have sufficient amount of mesopores.

Future work should be directed towards investigating the influence of additional variables, such as solvent type, cross-linker, monomer types and initiator concentrations on monolith chromatography. After a broad screening process the variables that are most influential on the response factor would be selected for further study. Such models will aid in the discovery of columns that are better suited for bio-fluid analysis intended for diagonstic purposes using chemometrics.

Over a decade ago CEC emerged as a technique that promised the selectivity of HPLC combined with the high efficiency of CE. The lack of dedicated commercial equipment and niche applications where established methods fail has restricted the use of CEC. The monolithic columns are a definite improvement over the packed-capillary technology but this advancement has not been sufficient to further commercial development. New achievements are targeted towards the discovery of novel columns with better selectivity and reproducibility that are suitable for separations of complex mixtures, such as proteins and digests.

References

[1] Strain, H. H., *Journal of the American Chemical Society* 1939, *61*, 1292-1293.

[2] Strain, H. H., Sullivan, J. C., *Analytical Chemistry* 1951, *23*, 816-823.

[3] Pretorius, V., Hopkins, B. J., Schieke, J. D., *Journal of Chromatography A* 1974, *99*, 23-30.

[4] Jorgenson, J. W., Lukacs, K. D., *Journal of Chromatography A* 1981, *218*, 209-216.

[5] Svec, F., Majors, R. E., *LC-GC North America* 2009, *27*, 1032-1039.

[6] Svec, F., *ELECTROPHORESIS* 2009, *30*, S68-S82.

[7] Svec, F., Peters, E. C., Sýkora, D., Fréchet, J. M. J., *Journal of Chromatography A* 2000, *887*, 3-29.

[8] in: Atlas, S. (Ed.), *Magnetic resonance imaging of the brain and spine*, Lippincott Williams & Wilkins, Philadelphia 2009.

[9] Remcho, V. T., *The Chemical Educator* 1997, *2*, 1-16.

[10] *Journal of the American Chemical Society* 2001, *123*, 10427-10427.

[11] *Capillary Electrochromatography*, Royal Society of Chemistry, Cambridge 1992.

[12] Nguyen, A., Moini, M., *Analytical Chemistry* 2008, *80*, 7169-7173.

[13] Knox, J., *Chromatographia* 1988, *26*, 329-337.

[14] Bartle, K. D., Carney, R. A., Cavazza, A., Cikalo, M. G., Myers, P., Robson, M. M., Roulin, S. C. P., Sealey, K., *Journal of Chromatography A* 2000, *892*, 279-290.

[15] Deyl, Z., Svec, F. eds., *Capillary Electrochromatography*, Elsevier, Amsterdam 2001.

[16] Bartle, K. D., Myers, P., *Journal of Chromatography A* 2001, *916*, 3-23.

[17] Choudhary, G., Horváth, C., *Journal of Chromatography A* 1997, *781*, 161-183.

[18] Wan, Q.-H., *Analytical Chemistry* 1997, *69*, 361-363.

[19] Snyder, L. R., Kirkland, J.J., Glajch, J.L., *Practical HPLC method development*, John Wiley & Sons 1997.

[20] Knox, J. H., *Journal of Chromatography A* 1999, *831*, 3-15.

[21] Rathore, A. S., Horváth, C., *Analytical Chemistry* 1998, *70*, 3271-3274.

[22] Pesek, J. J., Matyska, M. T., Dawson, G. B., Chen, Boysen, R. I., Hearn, M. T. W., *Analytical Chemistry* 2003, *76*, 23-30.

[23] Dong, X., Wu, R. a., Dong, J., Wu, M., Zhu, Y., Zou, H., *ELECTROPHORESIS* 2009, *30*, 141-154.

[24] Hilder, E. F., Svec, F., Fréchet, J. M. J., *ELECTROPHORESIS* 2002, *23*, 3934-3953.

[25] Eeltink, S., Svec, F., *ELECTROPHORESIS* 2007, *28*, 137-147.

[26] Ngola, S. M., Fintschenko, Y., Choi, W.-Y., Shepodd, T. J., *Analytical Chemistry* 2001, *73*, 849-856.

[27] Bandilla, D., Skinner, C. D., *Journal of Chromatography A* 2004, *1044*, 113-129.

[28] Lin, W., *Department of Chemistry and Biochemistry*, Concordia University, Montreal 2009.

[29] Lewis, F. D., Lauterbach, R. T., Heine, H. G., Hartmann, W., Rudolph, H., *Journal of the American Chemical Society* 1975, *97*, 1519-1525.

[30] Progent, F., Augustin, V., Tran, N. T., Descroix, S., Taverna, M., *ELECTROPHORESIS* 2006, *27*, 757-767.

[31] Archie, G. E., *Trans. AIME* 1942, *146*, 54.

[32] Gusev, I., Huang, X., Horváth, C., *Journal of Chromatography A* 1999, *855*, 273-290.

[33] Rathore, A. S., Wen, E., Horváth, C., *Analytical Chemistry* 1999, *71*, 2633-2641.

[34] Svec, F., Frechet, J. M. J., *Macromolecules* 1995, *28*, 7580-7582.

[35] Svec, F., Frechet, J. M. J., *Chemistry of Materials* 1995, *7*, 707-715.

[36] Lu, M., Feng, Q., Lu, Q., Cai, Z., Zhang, L., Chen, G., *ELECTROPHORESIS* 2009, *30*, 3540-3547.

[37] Eeltink, S., Herrero-Martinez, J. M., Rozing, G. P., Schoenmakers, P. J., Kok, W. T., *Analytical Chemistry* 2005, *77*, 7342-7347.

[38] Viklund, C., Svec, F., Frechet, J. M. J., Irgum, K., *Chemistry of Materials* 1996, *8*, 744-750.

[39] Viklund, C., Ponten, E., Glad, B., Irgum, K., Horstedt, P., Svec, F., *Chemistry of Materials* 1997, *9*, 463-471.

[40] Jiang, T., Jiskra, J., Claessens, H. A., Cramers, C. A., *Journal of Chromatography A* 2001, *923*, 215-227.

[41] Leardi, R., *Anal Chim Acta* 2009, *652*, 161-172.

[42] Araujo, P. W., Brereton, R. G., *TrAC Trends in Analytical Chemistry* 1996, *15*, 26-31.

[43] Araujo, P. W., Brereton, R. G., *TrAC Trends in Analytical Chemistry* 1996, *15*, 63-70.

[44] Araujo, P. W., Brereton, R. G., *TrAC Trends in Analytical Chemistry* 1996, *15*, 156-163.

[45] Kramer, R., *Chemometric Techniques for Quantitative Analysis*, Marcel Dekker, New York 1998.

[46] Cabral, J.-L., Bandilla, D., Skinner, C. D., *Journal of Chromatography A* 2006, *1108*, 83-89.

[47] Al-Bokari, M., Cherrak, D., Guiochon, G., *Journal of Chromatography A* 2002, *975*, 275-284.

[48] Jancŏ, M., Xie, S., Peterson, D. S., Allington, R. W., Svec, F., Fréchet, J. M. J., *Journal of Separation Science* 2002, *25*, 909-916.

[49] Rohr, T., Hilder, E. F., Donovan, J. J., Svec, F., Fréchet, J. M. J., *Macromolecules* 2003, *36*, 1677-1684.

[50] Jalili, N., Laxminarayana, K., *Mechatronics* 2004, *14*, 907-945.

[51] Kornysova, O., Surna, R., Snitka, V., Pyell, U., Maruska, A., *Journal of Chromatography A* 2002, *971*, 225-235.

[52] De La Rue, R. E., Tobias, C. W., *Journal of The Electrochemical Society* 1959, *106*, 827-833.

[53] Huang, X., Horváth, C., *Journal of Chromatography A* 1997, *788*, 155-164.

[54] Cabral, J.-L., *Department of Chemistry*, Concordia University, Montreal 2008, p. 275.

[55] Decker, C., Decker, D., Morel, F., *Photopolymerization*, American Chemical Society 1997, pp. 63-80.

[56] Ueki, Y., Umemura, T., Iwashita, Y., Odake, T., Haraguchi, H., Tsunoda, K.-i., *Journal of Chromatography A* 2006, *1106*, 106-111.

[57] Davies, M. P., De Biasi, V., Perrett, D., *Analytica Chimica Acta* 2004, *504*, 7-14.

[58] Iqbal, A., Khan, A.,, *Am. J. Eng. Appl. Sci.* 2010, *3*, 611-619.

[59] Niedz, R. P., Hyndman, S. E., Evens, T. J., *Scientia Horticulturae* 2007, *112*, 349-359.

[60] Gomase, V. S., Kale, K. V., Tagore, S., Hatture, S. R., *Current drug metabolism* 2008, *9(3)*, 213-220.

[61] Sleno, L., Emili, A., *Current Opinion in Chemical Biology* 2008, *12*, 46-54.

[62] Ngola, S. M., Fintschenko, Y., Choi, W. Y., Shepodd, T. J., *Analytical Chemistry* 2001, *73*, 849-856.

[63] Bandilla, D., Skinner, C. D., *Journal of Chromatography A* 2003, *1004*, 167-179.

[64] Bandilla, D., *Department of Chemisty and Biochemistry*, Concordia University, Montreal 2004.

[65] Rassi, Z. E., *Electrophoresis* 2010, *31*, 174-191.

Appendix A: Matrix Method for Determination of b Coefficients

The model matrix below has a set of eight points for each column and each set contains four -1 and four +1. The computation of each of the coefficients is the difference of two averages, the first average is the set of four experiments at the low level (-1), and the second average is that of the remaining four experiments (+1).

Table A-1 Model matrix and responses (Y) for the calculation of model coefficients (b_n) of 2^3

Run	b_0	b_1	b_2	b_3	b_{12}	b_{13}	b_{23}	b_{123}	Yield(Y_n)
1	+1	-1	-1	-1	+1	+1	+1	-1	55
2	+1	+1	-1	-1	-1	-1	+1	+1	53
3	+1	-1	+1	-1	-1	+1	-1	+1	50
4	+1	+1	+1	-1	+1	-1	-1	-1	40
5	+1	-1	-1	+1	+1	-1	-1	+1	49
6	+1	+1	-1	+1	-1	+1	-1	-1	46
7	+1	-1	+1	+1	-1	-1	+1	-1	56
8	+1	+1	+1	+1	+1	+1	+1	+1	49
b_n	**49.8**	**-2.8**	**-1.0**	**-0.3**	**-1.5**	**0.3**	**3.5**	**0.5**	

To estimate the linear term b_1 we have to multiply the b_1 coefficient by the response variable (Y) at its level (n) and divide the result by the number of experiments:

$$b_1 = \frac{\left(\sum b_{1,1}Y_1 + b_{1,2}Y_2 + \ldots + b_{1,8}Y_8\right)}{8} = \frac{\left(-55+53-50+40-49+46-56+49\right)}{8} = -2.8$$

Equation A_1 Calculation of the b_1 coefficient for a 2^3 factorial design model

This average is calculated for each of the variables tested. The interactive terms b_{12}, b_{13}, b_{23}, b_{123} in each row, are calculated as a product of their corresponding linear terms, *i.e.* $b_{12,n} = b_1 \times b_2 \times Y_n$. After calculation of all coefficients the general equation (Equation 15) becomes:

$$Yield = 49.8 - 2.8T - 1.0t - 0.3pH - 1.5T \times t + 0.3T \times pH + 3.5t \times pH + 0.5T \times t \times pH$$

Equation A_2 Model equation for the reaction yield

Appendix B: SEM Images of All 27 columns

SET 1 All 9 columns were synthesized at 0°C at 5K maginifcation

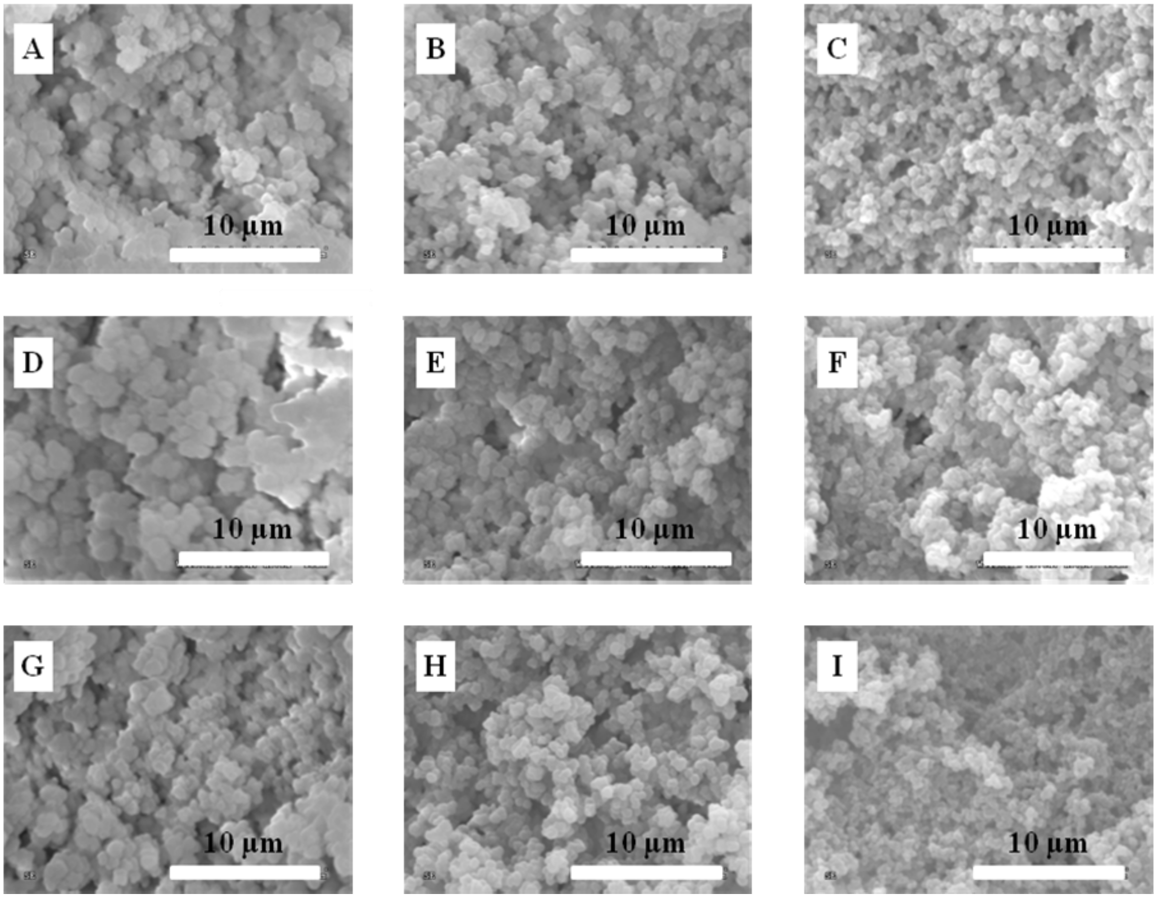

Figure B-1. A) 10 min; m:p = 1:2 B) 10 min m:p = 1:3 C) 10 min m:p = 1:4 D) 20 min; m:p = 1:2 E) 20 min m:p = 1:3 F) 20 min m:p = 1:4 G) 30 min; m:p = 1:2 H) 30 min m:p = 1:3 I) 30 min m:p = 1:4

SET 2 All 9 columns were synthesized at 20°C at 5K maginifcation

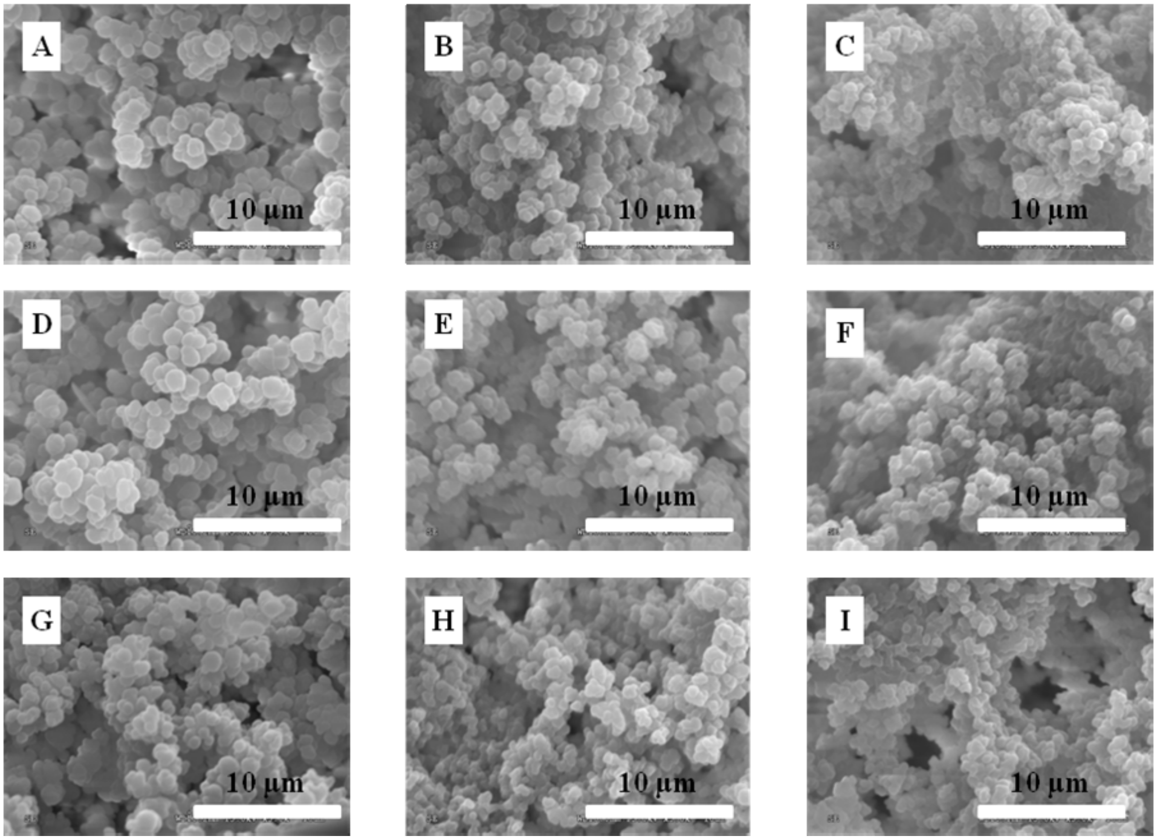

Figure B-2. A) 10 min; m:p = 1:2 B) 10 min m:p = 1:3 C) 10 min m:p = 1:4 D) 20 min; m:p = 1:2 E) 20 min m:p = 1:3 F) 20 min m:p = 1:4 G) 30 min; m:p = 1:2 H) 30 min m:p = 1:3 I) 30 min m:p = 1:4

SET 3 All 9 columns were synthesized at 40°C at 5K maginifcation

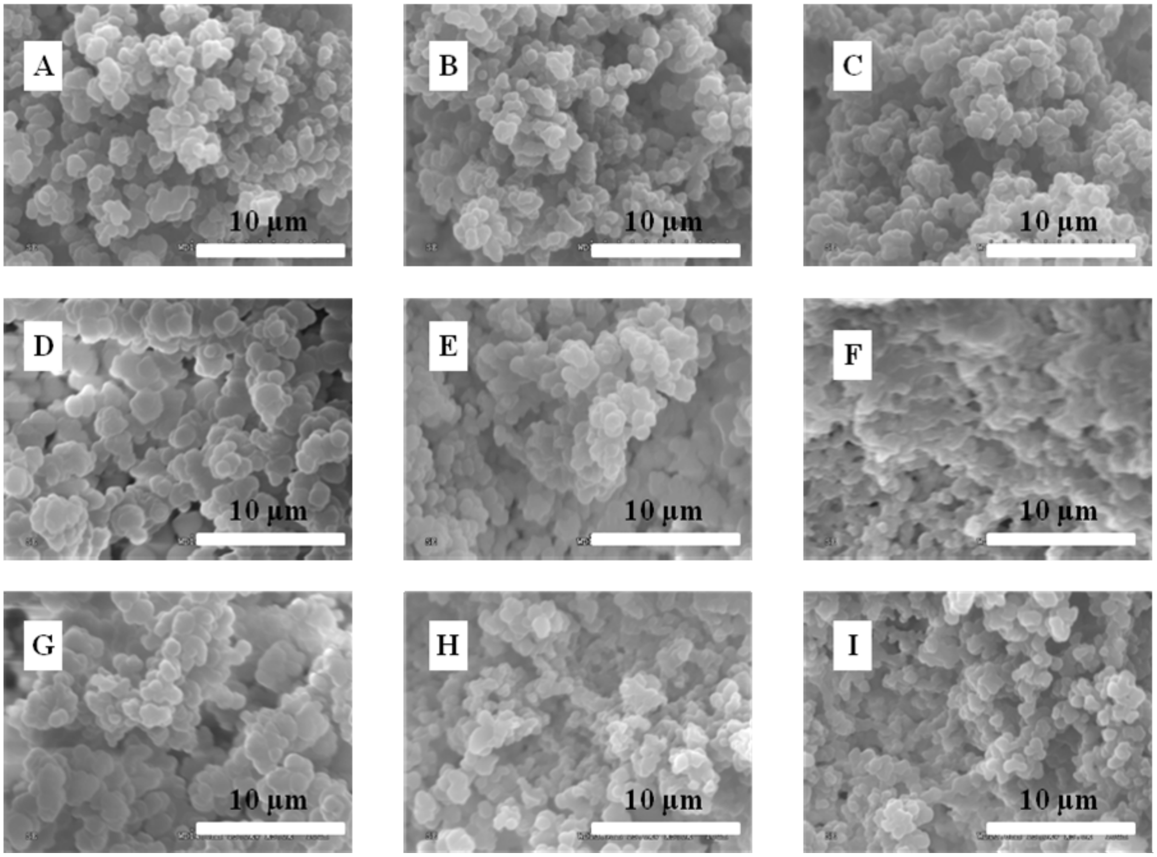

Figure B-3. A) 10 min; m:p = 1:2 B) 10 min m:p = 1:3 C) 10 min m:p = 1:4 D) 20 min; m:p = 1:2 E) 20 min m:p = 1:3 F) 20 min m:p = 1:4 G) 30 min; m:p = 1:2 H) 30 min m:p = 1:3 I) 30 min m:p = 1:4

Appendix C: SEM Images of UV Time Studies

All columns were synthesized at 20°C using m:p = 1:2 mix with a UV lamp with 1.8 W/cm^2 intensity

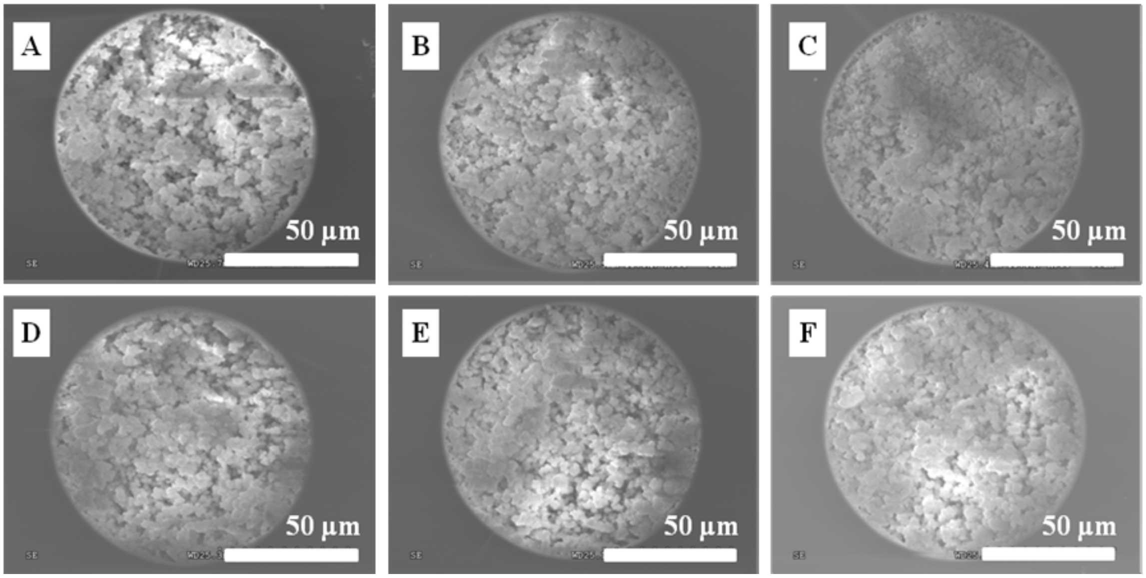

Figure C-1. A) 4 min B) 8 min C) 10 min D) 20 min; m:p = 1:2 E) 30 min F) 40 min